

# Development of a dynamic true triaxial electromagnetic Hopkinson bar system

Heping Xie<sup>1,2</sup>, Jianbo Zhu<sup>1,2</sup>\*, Yulong Li<sup>3</sup>, Tao Zhou<sup>1,2</sup>, Weiyue Bao<sup>1,2</sup>, Shiwei Zhang<sup>1,2</sup>, Zhongbin Tang<sup>3</sup>, Tao Suo<sup>3</sup>, Xiaoyong Song<sup>1,2</sup>, Jian Zhao<sup>4</sup>

- <sup>1</sup> State Key Laboratory of Intelligent Construction and Healthy Operation and Maintenance of Deep Underground Engineering, College of Civil and Transportation Engineering, Shenzhen University, Shenzhen, 518060, China
- <sup>2</sup> Guangdong Provincial Key Laboratory of Deep Earth Sciences and Geothermal Energy Exploitation and Utilization, Institute of Deep Earth Sciences and Green Energy, College of Civil and Transportation Engineering, Shenzhen University, Shenzhen, 518060, China
- <sup>3</sup> School of Aeronautics, Northwestern Polytechnical University, 127 Youyi West Road, Xi'an 710072, China
- <sup>4</sup> Department of Civil Engineering, Monash University, Melbourne, VIC 3800, Australia
- \* Corresponding authors; Emails: <u>jianbo.zhu@szu.edu.cn</u>

#### Peer review status:

This is a non-peer-reviewed preprint submitted to EarthArXiv.

This manuscript is to be submitted to the International Journal of Rock Mechanics and Mining Sciences.

#### 1 Development of a dynamic true triaxial electromagnetic Hopkinson bar system

- 2 Heping Xie<sup>1,2</sup>, Jianbo Zhu<sup>1,2</sup>\*, Yulong Li<sup>3</sup>, Tao Zhou<sup>1,2</sup>, Weiyue Bao<sup>1,2</sup>, Shiwei Zhang<sup>1,2</sup>, Zhongbin
- 3 Tang<sup>3</sup>, Tao Suo<sup>3</sup>, Xiaoyong Song<sup>1,2</sup>, Jian Zhao<sup>4</sup>
- 4 <sup>1</sup> State Key Laboratory of Intelligent Construction and Healthy Operation and Maintenance of Deep Underground
- 5 Engineering, College of Civil and Transportation Engineering, Shenzhen University, Shenzhen, 518060, China
- 6 <sup>2</sup> Guangdong Provincial Key Laboratory of Deep Earth Sciences and Geothermal Energy Exploitation and Utilization,
- 7 Institute of Deep Earth Sciences and Green Energy, College of Civil and Transportation Engineering, Shenzhen University,
- 8 Shenzhen, 518060, China

12

13

14

15

16

17

18

19

20

21

22

23

24

25

26

27

28

29

30

- <sup>9</sup> School of Aeronautics, Northwestern Polytechnical University, 127 Youyi West Road, Xi'an 710072, China
- 10 <sup>4</sup> Department of Civil Engineering, Monash University, Melbourne, VIC 3800, Australia
- \* Corresponding authors; Emails: jianbo.zhu@szu.edu.cn

**Abstract:** Subsurface rock masses and rock engineering are typically subjected to multiaxial static stresses, often superimposed by multidirectional dynamic disturbances induced by seismic events, blast loading and mechanical vibrations, etc. A comprehensive understanding of the dynamic mechanical behavior and failure mechanisms of rocks under such coupled multiaxial or threedimensional static and dynamic loading conditions is critical for the rational design, safe construction and long-term stability of rock engineering projects. However, there has been no three-dimensional dynamic theory of rock so far. A major reason is the lack of dynamic true triaxial apparatus, which is extremely difficult to develop using traditional techniques due to technical challenges such as precise and repeatable stress pulse generation, six-directional stress pulse synchronous loading, and triaxial static-dynamic coupled loading. To address this need, we developed a novel cutting-edge testing platform, i.e., dynamic true triaxial electromagnetic Hopkinson bar (DTEHB) system. It is the first apparatus in the world for studying dynamic responses of rock masses under coupled threedimensional dynamic disturbances (with strain rates ranging from 10<sup>1</sup> s<sup>-1</sup> to 10<sup>3</sup> s<sup>-1</sup>) and true triaxial static in situ stresses. The fundamental working principles, system configuration and key technical challenges overcome in the development of the DTEHB are introduced in detail in this paper. The system is comprised of the dynamic true triaxial Hopkinson bars, a triaxial/six-directional electromagnetic stress pulse synchronous loading system, a triaxial/six-directional static-dynamic coupling loading system, and a multivariate dynamic real-time data acquisition and analysis system. By combining electromagnetic energy conversion and synchronous control techniques, the DTEHB achieves highly repeatable (>99%) and precise true triaxial synchronous impact loading, and synchronous six-directional dynamic loading (time error ≤5 μs). The DTEHB system is also capable of simulating coupled triaxial/six-directional impact and static confining pressure loading, replicating 3D in situ stress conditions. Moreover, the system's reliability and performance are validated through analyzing controlled and adjustable stress waveforms (repeatability, duration, amplitude and arrival time), static true triaxial confining pressures and synchronous generation and arrival six-directional stress pulses. Dynamic true triaxial synchronized impact tests were successfully conducted on rock specimens for the first time. The establishment of the DTEHB could facilitate experimental testing of rock and other materials under a range of dynamic disturbances, thereby advancing the theory of three-dimensional rock dynamic theories.

**Keywords:** Rock dynamics; DTEHB; Dynamic true triaxial loading; Synchronous control

#### 1. Introduction

With increasing global demands for energy, resource exploitation, and transportation infrastructure, a growing number of rock engineering projects are being constructed-or planned-in deep underground environments characterized by high and complex crustal stresses, as well as active dynamic disturbances. In such settings, subsurface rock masses and engineered structures are subjected to true triaxial static stresses, often coupled with multi-directional dynamic loads induced by seismic activity, blasting, and mechanical vibrations. These combined static and dynamic stress conditions frequently lead to sudden and catastrophic dynamic failures, including rockbursts, coal bumps, and large-scale collapses, posing significant risks during both construction and operational phases (Ranjith et al. 2017; Rehbock-Sander and Jesel 2018; Xie et al. 2019, 2020). Given the severe hazards associated with such dynamic disasters and the challenges in their prediction and prevention, a thorough understanding of rock dynamic behavior-particularly under multi-axial static and dynamic loading conditions-is essential for ensuring the safety and stability of underground engineering projects.

Laboratory experimentation serves as a fundamental and widely adopted approach for investigating the dynamic mechanical and deformational behavior of rock materials under impact loading. Various experimental techniques have been developed to characterize rock dynamic responses across different strain rate regimes, including hydraulic/stress servo-controlled systems (Fairhurst and Hudson 1999; Olsson 1991), drop weight device (Reddish et al. 2005; Whittles et al. 2006), split Hopkinson pressure bar (SHPB) (Kolsky 1963; Zhao and Gary 1996) and planar impact machine (Ahrens and Rubin 1993). Among these, has emerged as the most prevalent method for dynamic rock testing at intermediate to high strain rates ( $10^{1}$ ~ $10^{3}$  s<sup>-1</sup>), owing to its well-established theoretical framework and experimental reliability.

The SHPB was first introduced by Kumar (1968) for characterizing the dynamic behavior of rocks and has since been widely employed in rock dynamics research (Doan and Gary 2009; Frew et al. 2001; Goldsmith et al. 1976; Ju et al. 2007; Lambert and Ross 2000; Li et al. 2005, 2017a, 2017b; Lindholm et al. 1974; Lu et al. 2010; Melosh et al. 1992; Olsson 1991; Perkins et al. 1970; Qi et al. 2019; Wang et al. 2009, 2017, 2018; Wu et al. 2016; Xia and Yao 2015; Xie and Sanderson 1996; Yuan et al. 2011; Zhang and Zhao 2013, 2014; Zhou et al. 2018, 2020; Zhu et al. 2018a). These studies

have established that the mechanical response and fracture mechanisms of rock materials are strongly strain-rate dependent. However, as noted earlier, rock masses in engineering settings are typically subjected to combined static in situ stresses and dynamic disturbances, a loading condition that conventional SHPB systems cannot replicate. To overcome this limitation, several modifications to the SHPB have been proposed in recent years. In a pioneering study, Li et al. (2008) developed an axisymmetric triaxial confined SHPB, enabling dynamic loading along one axis while maintaining static confining pressures ( $\sigma_1 \ge \sigma_2 = \sigma_3 \ne 0$ , where  $\sigma_1$ ,  $\sigma_2$  and  $\sigma_3$  are principal stresses). An alternative approach involves the use of a transverse constraint ring to achieve axisymmetric confinement during axial dynamic loading (Chen and Ravichandran 1997; Chen and Song 2011). For more complex stress states, Zhao and Cadoni (2009) conceptualized a modified SHB capable of imposing a static true triaxial stress ( $\sigma_1 \ge \sigma_2 \ge \sigma_3 \ne 0$ ) before dynamic impact along one direction. In a recent development, Liu et al. (2019) successfully constructed a triaxial Hopkinson bar and investigated the dynamic behavior of sandstone specimens under combined static true triaxial confinement and dynamic loading from a single direction.

However, none of the existing SHPB systems are capable of conducting dynamic tests under true triaxial impact conditions. In fact, rocks and rock-like materials may encounter complex multi-axial and multi-directional impacts, which can be either synchronous or asynchronous, with equal or unequal magnitudes in different directions. For example, during shaft excavation and mining operations employing the drill-and-blast method, rocks situated near the center of spirally arranged boreholes are often subjected to multidirectional blasting waves (e.g., symmetric, biaxial/four-directional, or triaxial/six-directional) that arrive at different times and exhibit directional variability. Similarly, in scenarios involving ballistic impact and penetration, protective rock and concrete structures are exposed to multiaxial dynamic loading (Karinski et al. 2017; Luo et al. 2019). Therefore, it is essential to develop an advanced dynamic testing system capable of applying controlled true triaxial impacts to rock specimens under laboratory conditions.

This paper presents the development of a dynamic true triaxial electromagnetic Hopkinson bar (DTEHB) system, designed to serve as an innovative experimental platform for investigating rock dynamic behavior under coupled three-dimensional (3D) dynamic disturbances and in-situ static stresses, with strain rates spanning  $10^1 \, \text{s}^{-1}$  to  $10^3 \, \text{s}^{-1}$ . The system's fundamental working principles, structural configuration, and key technical challenges encountered during its development are

- introduced in detail. Experimental validation confirms the system's reliability and effectiveness in
- 2 simulating true triaxial dynamic loading conditions. The successful implementation of the DTEHB
- 3 system advances the understanding of 3D rock dynamics and enhances its practical applications in
- 4 geotechnical engineering.

## 2. State-of-the-Art of Split Hopkinson Bar

A conventional SHPB system consists of four primary components: a striker, an input bar, an output bar and a buffer bar. During testing, the specimen is positioned between the input and output bars. In a typical experimental configuration, the test specimen is sandwiched between the incident and transmitter bars. When the striker impacts the free end of the input bar, it generates a longitudinal stress wave, which propagates along the input bar. Upon reaching the bar-specimen interface, the incident wave undergoes partial transmission through the specimen into the output bar (transmitted wave) and partial reflection back into the input bar (reflected wave). The dynamic strain response of the bars is typically monitored using resistance strain gauges bonded to the surfaces of the input and output bars. Provided that dynamic force equilibrium is achieved across both ends of the specimen, the dynamic stress, strain, and strain rate histories of the specimen can be derived based on one-dimensional elastic stress wave theory and the standard data reduction methodology recommended by the ISRM (Zhou et al. 2012).

Although the SHPB technique has been widely employed for dynamic testing of various materials, it remains an approximation rather than an ideal solution due to several inherent limitations. A fundamental assumption of the SHPB method is that the specimen must achieve dynamic stress equilibrium and undergo uniform deformation (Chen and Song 2011; Kolsky 1963). However, deviations from stress equilibrium can induce inertial stresses, which distort the amplitude of the transmitted wave recorded in the output bar. In brittle materials such as rocks and concrete, dynamic compression under non-equilibrium conditions may lead to premature failure at very low strains, significantly attenuating the transmitted wave signal (Lindholm et al. 1974). To mitigate these issues, pulse shaping techniques are commonly employed to transform the conventional trapezoidal incident pulse into a half-sine wave with a gradual rise time, thereby promoting stress equilibrium within the specimen (Frew et al. 2002; Li et al. 2009; Song and Chen 2004). Nevertheless, complete stress

equilibrium remains elusive, as the incident pulse must propagate through the specimen to establish uniform stress distribution (Frew et al. 2002). Additionally, conventional pneumatic launching systems-along with the challenges associated with precise pulse shaping-introduce inherent variability in incident pulse profiles, even under identical gas pressure conditions. This lack of repeatability further complicates the interpretation of dynamic test results.

In conventional SHPB testing, the incident stress pulse is typically generated through mechanical means, such as striker impact (Chen and Song 2011) or the sudden release of a pre-tensioned bar section (Cadoni et al. 2009). However, these methods face significant limitations in generating multiple synchronized incident stress pulses, which are essential for multi-axial and multi-directional dynamic testing. As a consequence, most existing SHPB systems are restricted to uniaxial dynamic loading. A notable advancement was reported by Nie et al. (2018b), who developed a symmetrically loaded SHPB apparatus utilizing electromagnetic energy conversion, enabling synchronous bidirectional compression or tension testing.

The majority of so-called triaxial SHPB systems can only apply axisymmetric triaxial confinement ( $\sigma_1 > \sigma_2 = \sigma_3 \neq 0$ ) to test specimens (Chen and Song 2011; Frew et al. 2002; Gran et al. 1989; Gary and Bailly 1998; Hokka et al. 2016; Li et al. 2008; Nemat-Nasser et al. 2000; Yuan et al. 2011; Peng et al. 2019). A key exception is the true triaxial compressed SHPB proposed by Zhao and Cadoni (2009) and further developed at Monash University (Zhao et al., 2015; Liu et al., 2019), which can apply independent triaxial static confining pressures. Furthermore, as underground engineering ventures into greater depths, rocks are increasingly subjected to thermo-mechanical coupling effects. However, no existing laboratory apparatus has been developed to study the coupled effects of real-time thermal treatment and dynamic and static triaxial stresses.

It is therefore essential to develop an innovative 3D dynamic testing device that is capable of repeatably generating stress waves with precise waveform control, accurately synchronizing multi-directional stress wave arrival times, and simulating the coupled effects of true triaxial synchronous impacts and *in situ* static stresses. Such an advancement would overcome the current constraints of SHPB technology and provide new insights into the dynamic behavior of rocks under complex loading environments.

## 3. Design and Configuration of the DTEHB System

To address the inherent limitations of conventional SHPB techniques and overcome critical challenges in characterizing three-dimensional dynamic responses and failure mechanisms in major rock engineering structures during construction and operation phases, this study presents an innovative development of the DTEHB system. The proposed system enables true triaxial dynamic loading with high-precision control, adjustable loading parameters, and reproducible stress waveforms. As illustrated in Fig. 1, the DTEHB system consists of four principal components: a main control system of the dynamic true triaxial Hopkinson bar, a triaxial/six-directional electromagnetic stress pulse synchronous loading system, a triaxial/six-directional static-dynamic coupling loading system, and a multivariate dynamic real-time data acquisition and analysis system. This advanced apparatus facilitates comprehensive investigations into the dynamic mechanical behavior and failure mechanisms of various materials—including rocks, hard soils, concrete, ceramics, composites, polymers, energy-absorbing materials, and aerospace materials—under complex loading conditions. The system accommodates a wide range of dynamic impact scenarios, ranging from symmetric loading to biaxial/four-directional and triaxial/six-directional loading, while incorporating in situ stress conditions.

## 3.1 Principle of the DTEHB

Figure 2 illustrates a schematic diagram of the stress state and wave propagation within the triaxial bar system. The specimen is under a combined loading condition comprising static triaxial confining pressures ( $\sigma_x \neq \sigma_y \neq \sigma_z \neq 0$ ) and dynamic true triaxial impacts. Notably, the static triaxial confining stresses are loaded to the specimen before applying dynamic true triaxial impacts. As depicted in Fig. 2, the stress waves generated during the true triaxial impact test (i.e.,  $\varepsilon_{x-inc}$ ,  $\varepsilon_{y-inc}$  and  $\varepsilon_{z-inc}$ ) propagate synchronously and symmetrically along the corresponding bars and through the specimen. Under synchronous and symmetrical six-directional impact loading, three distinct stress waves—reflected waves, transmitted waves and elastic waves induced by Poisson's effect—are generated along each principal axis. Although these three waves superimpose into a single resultant waveform, the propagation of the superposed wave in each axial direction still follows the one-dimensional elastic wave propagation theory (Cadoni and Albertini 2011). Moreover, the symmetric

propagation of two identical stress waves ensures dynamic force equilibrium along the loading direction throughout the impact process. Consequently, the one-dimensional elastic wave propagation theory remains applicable for analyzing the dynamic response of the specimen under true triaxial impact loading conditions.

To further clarify wave propagation in the DTEHB system, Fig. 3 presents an x-t diagram depicting wave propagation along the x-axis under symmetric loading conditions. Two identical incident waves propagate simultaneously and symmetrically from the ends of the right and left incident bars toward the specimen. Herein, the incident waves originating from the right and left bars are defined as  $\varepsilon_{inc\_right}$  and  $\varepsilon_{inc\_left}$ , respectively. In general, when a stress wave encounters the barspecimen interface, a portion transmits through the specimen into the output bar, while the remaining portion reflects back into the input bar. As shown in Fig. 3, upon reaching the right bar-specimen interface, the right-propagating wave partially reflects while the transmitted component propagates through the specimen into the left input bar. Similarly, the left-propagating wave follows an analogous transmission-reflection mechanism. Given that the wave transit time through the specimen is negligible compared to the incident wave duration, the initial wave arriving at the right input bar represents a superposition of the reflected component from the right incident wave and the transmitted component from the left incident wave, denoted as  $\varepsilon_{ref\_right}$ . An analogous superposition occurs in the left input bar, yielding  $\varepsilon_{ref\_teft}$ .

To avoid superposition of the incident and reflected waves in each bar, the two pulses are recorded by the resistance strain gauges mounted at midpoints of the bars. Since the square bars exhibit slenderness and the incident waveform approximates a half-sine pulse with minimal high-frequency content, waveform dispersion and oscillations are considered negligible. Therefore, in accordance with one-dimensional stress wave theory (Kolsky 1963), the dynamic forces (P) and particle velocities (V) at the right and left ends of the specimen can be calculated as follows:

$$P_{left} = AE(\varepsilon_{inc\_left} + \varepsilon_{ref\_left}), \quad P_{right} = AE(\varepsilon_{inc\_right} + \varepsilon_{ref\_right})$$
(1)

$$V_{left} = C(\varepsilon_{inc\_left} - \varepsilon_{ref\_left}), \quad V_{right} = C(-\varepsilon_{inc\_right} + \varepsilon_{ref\_right})$$
 (2)

where *C*, *A* and *E* are the P-wave velocity, cross-section area and elastic modulus of the input bar, respectively.

Under symmetric loading conditions with identical incident waves from both the right and left

- sides, dynamic stress equilibrium can be effectively maintained throughout the loading process.
- 2 Consequently, the dynamic stress within the specimen can be represented by the average stress
- 3 measured on its two boundaries. In accordance with one-dimensional stress wave theory (Kolsky
- 4 1963), the dynamic stress  $\sigma(t)$ , strain rate  $\dot{\varepsilon}(t)$  and dynamic strain  $\varepsilon(t)$  of the specimen under
- 5 dynamic impact loading along each axial direction can be computed as follows (Nie et al. 2018b; Xie
- 6 et al. 2021):

12

13

14

15

16

17

18

19

$$\sigma(t) = \frac{\sigma_{left} + \sigma_{right}}{2} = \frac{1}{2} \frac{A}{A_s} E(\varepsilon_{inc\_left} + \varepsilon_{inc\_right} + \varepsilon_{ref\_left} + \varepsilon_{ref\_right})$$
(3)

$$\dot{\varepsilon}(t) = \frac{V_{left} - V_{right}}{L_s} = \frac{C}{L_s} \left( \varepsilon_{inc\_left} + \varepsilon_{inc\_right} - \varepsilon_{ref\_left} - \varepsilon_{ref\_right} \right) \tag{4}$$

$$\varepsilon(t) = \int_0^t \dot{\varepsilon} dt = \frac{C}{L_s} \int_0^t (\varepsilon_{inc\_left} + \varepsilon_{inc\_right} - \varepsilon_{ref\_left} - \varepsilon_{ref\_right}) dt$$
 (5)

where  $L_s$  and  $A_s$  are the length and cross-section area of the specimen, respectively.

The strength of rock and rock-like materials exhibits a significant increase with elevated confining pressure (Patton et al. 1998; Richter et al. 2018; Wasantha and Ranjith 2014; Zhu et al. 2016). Moreover, under high confining pressure conditions, brittle failure transitions to ductile deformation (Kumari et al. 2017; Peng et al. 2015; Scott and Nielsen 1991). Given these mechanical responses, the von Mises stress criterion may be adopted to evaluate the dynamic deformation and failure behavior of specimens subjected to coupled dynamic true triaxial impacts and static triaxial stresses. The equivalent stress ( $\bar{\sigma}$ ) and equivalent strain ( $\bar{\varepsilon}$ ) of the specimen under the combined influence of triaxial static pressures and dynamic true triaxial impacts can be calculated as follows (Xu et al. 2020):

$$\bar{\sigma} = \sqrt{\frac{1}{2} \left[ (\sigma_{x\_dyn} + \sigma_{x\_static} - \sigma_{y\_dyn} - \sigma_{y\_static})^2 + (\sigma_{y\_dyn} + \sigma_{y\_static} - \sigma_{z\_dyn} - \sigma_{z\_static})^2 + (\sigma_{z\_dyn} + \sigma_{z\_static} - \sigma_{x\_dyn} - \sigma_{x\_static})^2 \right]} \quad (6)$$

$$\overline{\varepsilon} = \sqrt{\frac{2}{9} \left[ (\varepsilon_{x\_dyn} + \varepsilon_{x\_static} - \varepsilon_{y\_dyn} - \varepsilon_{y\_static})^2 + (\varepsilon_{y\_dyn} + \varepsilon_{y\_static} - \varepsilon_{z\_dyn} - \varepsilon_{z\_static})^2 + (\varepsilon_{z\_dyn} + \varepsilon_{z\_static} - \varepsilon_{x\_dyn} - \varepsilon_{x\_static})^2 \right]}$$
 (7)

where  $\sigma_{i\_dyn}$ ,  $\sigma_{i\_static}$ ,  $\varepsilon_{i\_dyn}$  and  $\varepsilon_{i\_static}$  represent dynamic stress, static confining pressure, dynamic strain and static strain corresponding to the peak static confining pressure along the *i*-axis (*i*=*x*, *y*, and

24 z).

#### 3.2 Configuration of the DTEHB

1

2

3

4

5

6

7

8

9

10

11

12

13

14

15

16

17

18

19

20

21

22

23

24

25

26

27

28

29

As aforementioned, the DTEHB is able to realize multi-axial and multi-directional synchronous or asynchronous loading (e.g., from 1D symmetric loading to biaxial/four-directional and triaxial/six-directional loading), dynamic-static coupled loading, controllable and repeatable dynamic impact. As illustrated in Fig. 1, the DTEHB consists of a main control system of the dynamic true triaxial Hopkinson bar, a triaxial/six-directional electromagnetic stress pulse synchronous loading system, a triaxial/six-directional static-dynamic coupling loading system, and a multivariate dynamic real-time data acquisition and analysis system.

The main control system of the dynamic true triaxial Hopkinson bar comprises three components: the primary structural frame of the triaxial Hopkinson bar, a 3D alignment and leveling device for precise triaxial Hopkinson bars and specimen positioning, and an energy-absorbing buffer with selfresetting capability. The benchmark platform provides support and reference plane for the whole system. The primary structural frame is a 3D symmetric frame structure with sufficiently high stiffness. To achieve true triaxial loading, the Hopkinson bar is designed with a square cross-section. In the DTEHB, three pairs of orthogonal square bars with circular bulges constitute the 3D dynamic impact loading bar system, as shown in Fig. 2. Fig. 1(b) illustrates three key components of the 3D centering and leveling system: the benchmark box, serving as the reference datum for aligning the triaxial Hopkinson bars; the 3D adjustment and support device for Hopkinson bars, enabling precise angular control of each square bar; and the pitch adjustment device of the electromagnetic stress pulse generator, which ensures optimal alignment and leveling between the bar and the pulse generator. The coordinated operation of these subsystems ensures precise coaxial alignment among the specimen, Hopkinson bars, and pulse generators—a fundamental prerequisite for achieving reliable and repeatable experimental results under dynamic true triaxial loading conditions. The energy-absorbing buffer incorporates a self-resetting mechanism designed to minimize the gap between the Hopkinson bar and the electromagnetic stress pulse generator while enhancing the efficiency of dynamic load absorption. A detailed description of the energy-absorption buffer and self-resetting device is provided in Section 4.2.3.

The triaxial/six-directional electromagnetic stress pulse synchronous loading system consists of two key components: an electromagnetic stress pulse generation system and a triaxial/six-directional

electromagnetic stress pulse synchronized control system (SCS). In this system, electrical energy is converted into electromagnetic pulses via the coordinated operation of electromagnetic stress pulse generators (ESPGs) and the SCS, with the resulting stress waves transmitted through elastic bars to the tested specimen. The pulse duration and amplitude can be precisely controlled by adjusting the capacitance and charging voltage of the ESPGs. Additionally, the high-precision SCS ensures the stability and repeatability of the generated electromagnetic stress pulses. Moreover, the SCS facilitates the synchronous generation of electromagnetic stress pulses across multiple ESPGs, thereby enabling multi-axial and multi-directional synchronous dynamic loading under various loading conditions—including uniaxial symmetric loading, biaxial/four-directional loading, and triaxial/six-directional loading—in either synchronous or asynchronous modes.

The triaxial/six-directional static-dynamic coupling loading system consists of three primary components: a hydraulic servo-controlled confining pressure loading subsystem, a confining pressure loading apparatus, and a triaxial bar assembly with circular bulges. The confining pressure loading subsystem employs hydraulic servo-controlled technology to apply true triaxial static stresses to the specimen, with the capability to independently regulate each principal stress component to either identical or varying magnitudes, thereby accurately replicating in situ static stress conditions. A feature of the servo-controlled system is its ability to maintain the true triaxial static confining pressure at a near-constant level during testing. This ensures stability by effectively mitigating pressure oscillations that would otherwise arise due to the Poisson effect under dynamic loading.

Accurate acquisition and analysis of experimental data are critical in dynamic testing, as the validity of results hinges on the precise capture and isolation of true specimen responses from surrounding noise. Reliable measurement of dynamic mechanical characteristics, such as strain signals, acoustic emissions, and fracture evolution, is essential for understanding rock behavior under dynamic loading. To address this requirement, the DTEHB integrates multiple advanced techniques, combining contact and non-contact measurement methods, real-time monitoring, post-test analysis, and macro- to micro-scale characterization using both nondestructive and destructive approaches. These methods collectively enable comprehensive observation, data collection, and analysis of dynamic rock responses. Table 1 summarizes the instrumentation and techniques employed in the DTEHB, detailing their respective roles in data acquisition and analysis. Notably, digital image correlation and ultra-high-speed imaging are utilized to capture surface deformation and fracture

- dynamics under various loading conditions, such as uniaxial symmetric and biaxial/four-directional
- 2 dynamic loading. However, these optical techniques are not applicable in true triaxial dynamic
- 3 loading tests, where the specimen is fully confined by six opaque bars, preventing direct visual access
- 4 to the specimen's surface.

## 4 Technical Challenges Overcome in the Development of the DTEHB

To fulfill the functions of the DTEHB, several critical technical challenges have been resolved. High-precision stress wave generation: a novel technique has been developed to produce targeted stress waves with exceptional accuracy and repeatability. Synchronous multidirectional wave generation: an advanced methodology ensures the synchronous generation of multiple identical stress waves with high consistency. Precision-controlled multidirectional loading: a specialized technique enables the precise synchronization of stress wave loading from different axes, maintaining a time difference within the microsecond range. Dynamic triaxial impact coordination: an effective control system has been designed to coordinate the dynamic triaxial impact loading process. Servo-controlled static pressure loading: a servo-controlled triaxial static pressure loading system has been developed to apply in situ stresses.

### 4.1 Triaxial/Six-directional Electromagnetic Stress Pulse Synchronous Loading System

As aforementioned, conventional SHPB systems exhibit an inherent limitation in conducting high-precision, repeatable multi-axial and multi-directional dynamic loading tests under either synchronous or asynchronous conditions. This limitation arises primarily from the technical challenges associated with achieving microsecond-scale synchronization and generating controllable incident stress pulses with sufficient precision and repeatability when using traditional mechanical loading methods, such as striker impacts or the sudden release of pre-tensioned bar sections (Nie et al. 2018a; Cadoni and Albertini 2011). To overcome this challenge, this study introduces an innovative approach based on electromagnetic energy conversion technology, which enables the highly precise and repeatable generation of multiple identical and synchronized stress waves. The proposed SCS ensures accurate temporal coordination of stress wave generation and loading application. Furthermore, an automated control system governs the electromagnetic pulse generation mechanism, ensuring both operational precision and safety. The integration of these key

- 1 components—electromagnetic energy conversion, the SCS, and the automated control system—
- 2 facilitates the realization of controllable true triaxial dynamic loading conditions, thereby addressing
- 3 a critical gap in experimental rock mechanics.

#### 4.1.1 Electromagnetic Stress Pulse Generation Device

The proposed DTEHB system consists of three orthogonally arranged electromagnetic split Hopkinson bar assemblies, as illustrated in Fig. 1. Given that the structural configuration, operational principles, and loading mechanisms are identical along all three axes (X, Y, and Z), and that each axis operates independently without mutual interference, the following discussion focuses on the system's design and functionality along a single axis for brevity.

As depicted in Fig. 4, the single-axis bar system includes two ESPGs with active and inductive coils, two incident bars, and two symmetrically positioned charging circuits. Each charging circuit, regulated by a thyristor, is connected to its corresponding ESPG. The circuit incorporates a bridge rectifier and a high-power transformer to convert an alternating voltage input (380 V) into a high-voltage direct current (DC). A bank of pulse capacitors, configured in series or parallel, serves as an energy storage unit during charging. Together with the active coil of the ESPG and the thyristor, these components form an LC oscillation circuit. Upon triggering, the thyristors are simultaneously activated, allowing the discharge current from the fully charged capacitor banks to flow uniformly into the two active coils. The thyristors function as unidirectional switches, ensuring that only the forward discharge current propagates while blocking any reverse current. The pulsed current is then converted into a mechanical stress wave via electromagnetic induction. A detailed theoretical treatment of the electromagnetic conversion process is omitted here for conciseness, readers can refer to Nie et al. (2018a) for further information.

To obtain repeatable and precise electromagnetic stress pulses, it is imperative to meticulously design and fabricate the ESPG, with particular attention to its active coil. Figure 5 illustrates the structural and parametric design of a representative active coil. The coil features an outer diameter of 144 mm and a height of 58 mm, with its core comprising a 4-mm-thick and 15-mm-high copper strip wound in eight concentric layers in a Swiss roll configuration. To ensure machining accuracy and inductance consistency, the copper strips are precision-cut using wire electrical discharge machining. A 2-mm inter-turn gap is maintained between successive copper strip layers, filled with insulating

rubber to prevent interlayer discharge. Additionally, a high-strength composite base is incorporated to counteract the transient Lorentz forces acting perpendicular to the coil. Two protruding copper strips serve as the positive and negative electrodes, separated by an insulating block to avoid short-circuiting.

Upon fabrication, the inductance of the ESPG is determined, as it is inherently governed by the number of copper strip turns and remains fixed for a given generator (Nie et al., 2018a). Based on underdamped LRC circuit theory, the discharge current duration is primarily dictated by the active coil's capacitance and can be estimated as follows:

$$T = \pi \sqrt{LC_e} \tag{8}$$

where L and  $C_e$  are the inductance and capacitance of the active coil, respectively.

Based on the principle of electromagnetic conversion, the discharge current flowing into the active coil induces a time-dependent Lorentz force at the surface of the adjacent inductive coil, thereby generating a stress pulse. The duration of this stress pulse is intrinsically linked to the discharge current's transient duration, which is primarily governed by the capacitance of the active coil. By modifying the capacitance through the addition or removal of parallel or series-connected capacitors, a series of stress pulses with varying durations can be systematically generated.

Fundamentally, the energy released during capacitor discharge in an LC circuit is converted, via electromagnetic transduction, into the energy carried by the stress pulse. As a result, the amplitude of the electromagnetic stress pulse can be precisely controlled by adjusting the stored energy of the capacitor during the charging and discharging phases. According to LC circuit discharge theory, the electrical energy stored in the capacitor can be expressed as:

$$W_e = \frac{1}{2} C_e U^2 (9)$$

where U is the charging voltage.

The capacitor is employed to modulate the pulse duration, facilitating precise adjustment of the charging voltage in accordance with the desired pulse characteristics. This mechanism enables effective control over the pulse amplitude. In accordance with the specifications, the wave amplitude is designed to fall within the range of 0 to 600 MPa, while the wave duration is set to a range of 300 to 800  $\mu$ s.

#### 4.1.2 Synchronous Pulse Control System

As aforementioned, the true triaxial dynamic testing apparatus consists of three orthogonally arranged symmetric Hopkinson bars, with each bar subjected to independently generated electromagnetic stress pulses. The key requirement for achieving true triaxial dynamic impact loading is the synchronous generation of incident stress pulses along all three bars. The primary technical challenge, therefore, lies in ensuring precise temporal synchronization of these stress pulses.

Figure 6 illustrates the schematic of the synchronous control system. The charging circuit, comprising a transformer and a bridge rectifier, resembles that of a conventional uniaxial symmetric electromagnetic Hopkinson bar (SHB) system. Six parallel-connected capacitors are integrated into this circuit, each regulated by an independent switch. A digital delay generator (DG645), with nanosecond-level timing accuracy, and a multichannel high-voltage pulse trigger are employed to generate and coordinate independent triggering signals for the thyristors along each axis. This configuration ensures precise control over the initiation time of stress pulses in all three loading directions, achieving synchronization accuracy within 5 μs—a critical requirement for true triaxial impact loading.

During testing, once the preselected capacitors reach their target charge, the digital delay generator outputs triggering signals to the multichannel high-voltage pulse trigger at the predetermined time. The trigger then simultaneously activates the thyristors in the designated branches, inducing discharge currents that energize the ESPGs. Through electromagnetic conversion, synchronized stress pulses are generated. To further enhance synchronization accuracy, an energy-absorbing buffer with self-resetting capability was developed to ensure precise contact alignment between the electromagnetic stress pulse generators and the Hopkinson bars. This mechanism minimizes mechanical delays, contributing to the overall synchronization precision. Finally, the generated stress pulses propagate into the Hopkinson bars as incident waves, as shown in Fig. 2.

The synchronous discharge control system ensures the precise generation of electromagnetic stress pulses with high temporal coordination. When integrated with the self-resetting, energy-absorbing buffer of the dynamic loading system, it facilitates multiaxial and multidirectional synchronous impact loading with a time discrepancy of less than 5 µs.

#### 4.1.3 Central Control System

The synchronization of the dynamic triaxial impact loading system necessitates an advanced control system to ensure precise operation. As illustrated in Fig. 7, the control system comprises three primary modules: the human-machine interface (HMI) system, the charging and discharging system, and the dynamic testing system. During operation, the HMI system provides real-time monitoring of the system status and converts manual inputs into digital control signals. These signals are subsequently transmitted to the charging and discharging system, which regulates the charging or discharging of the capacitor bank. Upon discharge, the stored electrical energy is converted into electromagnetic energy within the dynamic testing system, generating incident stress waves that are utilized to characterize the dynamic response of the specimen.

The charging and discharging system constitute a critical component of the DTEHB. When a charging command is issued by the HMI system, the programmable logic controller (PLC) activates the charging circuit, establishing a connection with the capacitor bank. Concurrently, voltage and current transmitters continuously monitor the electrical parameters, converting them into analog signals that are relayed to the PLC via an Analog I/O module for real-time supervision. To ensure operational safety, an emergency monitoring mechanism is integrated into the system. For example, if overcharging or an excessive charging rate is detected, the PLC immediately terminates the charging process to prevent equipment damage. Upon receiving a discharge command, the PLC engages the discharging circuit, directing the stored energy from the capacitor bank to the ESPGs, thereby activating the dynamic testing system. In emergency scenarios, the PLC can bypass normal operation and safely dissipate the stored energy through a ground leakage trigger, protecting the system from potential hazards.

## 4.2Triaxial/Six-directional Static-Dynamic Coupling Loading System

In conventional axisymmetric triaxial confined SHPB apparatus, the applied static confining stress state ( $\sigma_1 > \sigma_2 = \sigma_3 \neq 0$ ) deviates from the true in-situ stress conditions ( $\sigma_1 > \sigma_2 > \sigma_3 \neq 0$ ). To overcome this limitation, a servo-controlled static triaxial pressure loading system has been developed. This system consists of a high-stiffness triaxial loading frame integrated with a servo-controlled hydraulic pressure loading system. A critical requirement is that the servo control system ensures minimal

fluctuation in static confining pressure during dynamic loading events. Furthermore, to achieve seamless coupling between static and dynamic triaxial loading, a dynamic-static coupling loading conversion control device has been designed. Additionally, to satisfy the demands of efficient energy absorption and high repeatability of electromagnetic stress pulses, an energy absorption buffer with self-resetting capability has been incorporated into the system.

#### 4.2.1 Servo-controlled static triaxial pressure loading device

As illustrated in Fig. 1, the loading frame consists of an orthogonal triaxial loading system. The supporting frame, fabricated from high-strength alloy steel (42CrMo) through precision machining, exhibits exceptional rigidity and mechanical strength. This triaxial frame not only supports the entire system's weight but also ensures a high-precision reference plane for accurate load application.

The servo-controlled hydraulic pressure system includes a hydraulic pump station, three independent hydraulic cylinders, and a servo control unit. The system is designed to deliver a maximum confining pressure of 300 MPa with a precision of  $\pm 0.5$  MPa. A schematic representation of the static confining pressure application along one principal axis is provided in Fig. 8. The hydraulic loading assembly for each axis comprises a hydraulic cylinder, a reference benchmark box, support frames, two confining pressure loading frames, and two square transmission bars.

#### 4.2.2 Static-dynamic coupling loading conversion device

The bar component consists of six square bars, each measuring  $50 \times 50 \times 2800 \text{ mm}^3$ . To minimize electromagnetic interference in strain signal detection, the square bar is made of antimagnetic titanium alloy with high yield strength (approximately 1050 MPa). Additionally, to mitigate stress wave dispersion and oscillation, the square bars are precision-machined to ensure a maximum straightness deviation of 0.1%, with surface grinding achieving a polishing flatness of 0.8. Since the incident end of the square bar interfaces directly with the ESPG—which cannot sustain prestress—applying static confining pressure directly at this end is infeasible. To overcome this limitation, a circular bulge ( $\emptyset$ 90 mm, thickness 70 mm) is integrated into the bar at a distance of 150 mm from the incident end, as shown in Fig. 8. This design allows the static confining pressure to be applied via the bulge rather than the bar's incident end. The static confining pressure is supplied by a servo-controlled hydraulic system (Fig. 8), transmitting the static confinement to the specimen through the bulge and adjacent bar segments.

All structural components, except the confining pressure loading frames and square bars, are bolted into a rigid, unified frame. During operation, the specimen is sandwiched between two square bars, with one end of the frame (right side in Fig. 8) fixed and the opposite end serving as the confining pressure loading end. A hydraulic pump station actuates a piston within the hydraulic cylinder, displacing the loading frame until it contacts the circular bulge. As the piston advances rightward, the loading frame transfers the axial load to the specimen via the bulge and the adjoining square bar. Crucially, the fixed right-side frame ensures that the right square bar and specimen face remain stationary throughout loading. Once the target confining pressure is attained, it is held constant for subsequent dynamic impact testing. During dynamic loading, the static confining pressure remains relatively stable to prevent fluctuations induced by the Poisson's effect, ensuring consistent boundary conditions.

#### 4.2.3 Energy absorption buffer with self-resetting capability

During testing, an initial gap might exist between the incident bar and the ESPG, which may distort the incident stress waveform. Furthermore, a portion of the incident energy remains in the bars after dynamic loading and propagates into the system frame, potentially compromising the structural integrity and long-term durability of the testing apparatus. To mitigate these issues, a stress pulse energy absorption buffer with self-resetting capability has been developed.

As illustrated in Fig. 9, the buffer consists of two compressible/extendible hydraulic cylinders and two high-capacity nitrogen springs (loading capacity: 600 MPa). These components work synergistically to absorb residual energy transferred from the bars, thereby safeguarding the testing system during dynamic loading. Notably, the hydraulic cylinders can be extended by increasing the intake air pressure, effectively eliminating the initial gap and ensuring waveform consistency in the incident stress pulse. Additionally, maintaining constant air pressure allows the cylinders to retract to their original position after each test, enabling automatic resetting for repeated experiments. To further enhance system stability, a linear guideway has been integrated beneath the ESPG, ensuring strictly linear displacement and preventing wave oscillations induced by lateral movement of the ESPG.

## 5 Verification and Testing

To validate the functionality and performance of the proposed DTEHB system, a series of experimental verification tests were conducted.

#### 5.1 Adjustability of stress wave duration

Figure 10 presents the incident stress waves with varying durations generated by the ESPG. By adjusting the capacitance of the capacitor bank—for example, increasing it from 1 mF to 4 mF—the pulse duration of the incident stress wave can be controlled within a range of 400 to 800 µs. It should be noted that the stored energy in the capacitor bank is governed by both the charging voltage and capacitance, as expressed in Eq. (9). Consequently, to maintain a consistent wave amplitude while varying pulse durations across different capacitances, the charging voltage must be correspondingly adjusted.

Additionally, as demonstrated in Fig. 9, the stress wave duration can be reduced to approximately 300 µs by decreasing the number of copper strip turns from 16 to 8. This effect arises from the inverse proportionality between the number of turns and the inductance of the active coil. A reduction in the number of turns lowers the coil inductance, thereby shortening the stress wave duration. Conversely, increasing the number of turns extends the wave duration due to the resultant increase in inductance.

## 5.2 Adjustability of stress wave amplitude

Figure 11a illustrates the influence of charging voltage on stress wave amplitude while maintaining a constant capacitance of 4 mF. As the charging voltage increases from 1500 V to 4000 V, the stress wave amplitude exhibits a corresponding increase from 100 MPa to 600 MPa, while the wave duration remains stable at approximately 725 μs. This demonstrates precise control over stress wave amplitude, fulfilling the requirements for diverse experimental conditions. It is noteworthy that stress wave amplitude can also be modulated by varying the capacitance and the number of turns in the active coil (Fig. 11b). Consequently, through systematic adjustment of capacitance, charging voltage, and active coil configuration, the desired stress wave duration and amplitude can be precisely tailored to meet specific testing requirements.

#### 5.3 Repeatability of stress waves

The reproducibility and reliability of experimental results critically depend on the repeatability of incident stress waves. Figure 12 presents the results of repeated incident stress wave generation using the same ESPG (with an active coil capacitance of 2 mF and 12 turns of copper tape) at two different charging voltages (1500 V and 2000 V). As illustrated in Fig. 12, the incident stress waves produced via electromagnetic conversion exhibit excellent repeatability in terms of wave amplitude, waveform shape, and duration, achieving a repeatability rate of ≥99%. These findings confirm that electromagnetic conversion technology provides a robust solution for generating highly repeatable incident stress waves, overcoming the limitations associated with traditional mechanical impact methods that rely on striker-bar collisions at the incident bar end.

#### 5.4 Static true triaxial confining pressures

The ability of the dynamic true triaxial Hopkinson bar to accurately apply independent triaxial static confining pressures is crucial for investigating the mechanical behavior of deep underground rocks under coupled true triaxial static confinement and dynamic disturbances. As demonstrated in Fig. 13, the static true triaxial confining pressure loading system successfully imposes independent static stresses along the X, Y, and Z axes. The results confirm that the DTEHB can apply static confining pressures smoothly and independently without cross-interference between axes. Moreover, the system maintains stable confining pressure upon reaching the target load, validating its effectiveness in simulating true triaxial static stress conditions.

#### 5.5 Dynamic true triaxial loading test

To verify the viability and effectiveness of the DTEHB, dynamic true triaxial loading tests were conducted on cubic coal and sandstone specimens. It should be noted that under dynamic true triaxial impact loading, volumetric compression inevitably occurs due to the compaction and collapse of pre-existing defects within the rock. Consequently, if the specimen dimensions match the cross-sectional side length of the square bars (50 mm), bar collision becomes unavoidable. To mitigate this issue, the specimen side length was increased by 1 mm, ensuring sufficient deformation space (up to 2% strain) while preventing bar interference, given that the dynamic deformation of brittle rocks typically

remains below 1%. Additionally, a 0.5 mm chamfer was incorporated at each edge of the cubic specimen to minimize geometric mismatch between the specimen and the loading surfaces.

Figure 14 demonstrates the results of a typical dynamic true triaxial impact test on a coal specimen. Fig. 14a shows the incident and reflected voltage signals recorded on three orthogonal sets of titanium alloy bars. The results demonstrate that the six independent ESPGs produce highly synchronized incident stress waves, with arrival time discrepancies of less than 5 μs and near-identical waveforms and pulse durations. The peak values of the six incident waves exhibit remarkable consistency (>99%), with the Z1 peak being only 1.89% higher due to a marginally greater discharge voltage (~10 V) in its corresponding capacitor. These findings confirm that the DTEHB can generate precisely synchronized multiaxial stress pulses, enabling uniform dynamic loading. The reflected waveforms, while generally consistent, show greater peak variability, primarily attributable to the anisotropic wave transmission and reflection properties of the rock.

Figure 14b illustrates the dynamic stress balance across the specimen along the X-, Y-, and Z-axes, derived from the stress waves in Fig. 13a. Dynamic stress balance is achieved when the stress difference between opposing specimen faces remains below 5%. The results indicate excellent stress equilibrium, with balanced durations covering 63–82% of the total stress wave duration in each direction. This effectively resolves the stress equilibrium limitations inherent in conventional SHPB systems.

Figure 14c depicts the dynamic stress-strain responses along the three principal axes. The curves exhibit similar evolutionary trends: an initial compaction phase followed by linear elastic deformation, a brief nonlinear regime, peak stress attainment, and post-peak rebound unloading. Despite nearly identical incident stresses in all directions (Fig. 13a), slight variations in peak stresses arise due to material heterogeneity. Notably, the peak strain in the Z direction is larger than that in the X and Y directions, predominantly attributable to the presence of anisotropy in the specimen, which gives rise to a comparatively larger strain in the Z direction.

## 6 Summary

This paper presents the development of a novel dynamic true triaxial electromagnetic Hopkinson bar (DTEHB) system, designed to investigate the dynamic behavior of rocks under coupled multiaxial static and dynamic loading conditions. The system comprises a main control system of the dynamic

true triaxial Hopkinson bar, a triaxial/six-directional electromagnetic stress pulse synchronous loading system, a triaxial/six-directional static-dynamic coupling loading system, and a multivariate dynamic real-time data acquisition and analysis system. The servo-controlled static triaxial confining pressure system enables independent application of true triaxial static stresses along three orthogonal directions. Electromagnetic energy conversion is employed to generate highly repeatable and precise stress pulses, while a synchronization control technique ensures that the time delay between multiple incident stress waves arriving at the specimen's loaded end face does not exceed 5 µs. An integrated control system coordinates the dynamic triaxial impact loading process, ensuring both operational safety and optimal performance of the DTEHB. By combining electromagnetic energy conversion and synchronous control techniques, the DTEHB achieves high-precision true triaxial synchronous impact loading. Moreover, the DTEHB system is capable of simulating coupled triaxial/six-directional impact and static confining pressure loading, replicating 3D in situ stress conditions—a capability beyond the reach of conventional SHPB apparatus.

The development of the DTEHB provides a cutting-edge dynamic testing platform for systematic study of dynamic behavior of rocks and other materials under 3D dynamic disturbances, with strain rate ranging from 10<sup>1</sup> s<sup>-1</sup> to 10<sup>3</sup> s<sup>-1</sup>), while accounting for in situ stress conditions. The anticipated findings derived from this system are expected to advance the theoretical framework of 3D rock dynamics and support practical applications in rock engineering.

## **CRediT** authorship contribution statement

Heping Xie: Writing - original draft, Conceptualization, Methodology, Investigation, Formal analysis, Funding acquisition. Jianbo Zhu: Methodology, Writing - review & editing, Investigation, Supervision, Funding acquisition. Yulong Li: Methodology, Writing - review & editing, Investigation, Supervision. Tao Zhou: Methodology, Writing - review & editing, Investigation, Supervision. Weiyue Bao: Methodology, Writing - review & editing, Investigation, Formal analysis. Shiwei Zhang: Methodology, Writing - review & editing, Formal analysis. Zhongbin Tang: Methodology, Writing - review & editing. Tao Suo: Methodology, Writing - review & editing. Xiaoyong Song: Methodology, Writing - review & editing. Jian Zhao: Methodology, Writing - review & editing.

## **Declaration of competing interest**

- 2 The authors declare that they have no known competing financial interests or personal
- 3 relationships that could have appeared to influence the work reported in this paper.

## 4 Acknowledgements

- 5 This research is financially supported by the Program for Guangdong Introducing Innovative
- and Entrepreneurial Teams (2019ZT08G315) and the National Natural Science Foundation of China
- 7 (52325404).

1

8

10

## Data availability

9 Data will be made available on request.

## Supplementary material

- A supplementary video is supplied for better understanding of the design, principle, function and
- 12 some potential applications of the DTEHB, and can be found online at
- 13 https://doi.org/10.6084/m9.figshare.11473737.v1.

## 14 References

- Ahrens TJ, Rubin AM. Impact-induced tensional failure in rock. J Geophys Res Planets. 1993;98(E1):1185-1203.
- 16 Cadoni E, Albertini C. Modified Hopkinson bar technologies applied to the high strain rate rock tests. Advances in
- 17 Rock Dynamics and Applications. edited by Y. X. Zhou, and J. Zhao, 2011:79-104.
- Cadoni E, Meda A, Plizzari GA. Tensile behaviour of FRC under high strain-rate. *Mater Struct*. 2009; 42(9):1283-
- 19 1294.
- 20 Chen WW, Ravichandran G. Dynamic compressive failure of a glass ceramic under lateral confinement. J Mech
- 21 *Phys Solids*. 1997;45(8):1303-1328.
- 22 Chen WW, Song B. Split Hopkinson Kolsky bar: design, testing and applications. Springer Science and Business
- 23 Media. 2011.
- Doan ML, Gary G. Rock pulverization at high strain rate near the San Andreas fault. Nat Geosci. 2009;2(10): 709-
- 25 712.
- 26 Fairhurst CE, Hudson JA. Draft ISRM suggested method for the complete stress-strain curve for intact rock in
- 27 uniaxial compression. Int J Rock Mech Min Sci. 1999;36(3):279-289.
- 28 Frew DJ, Forrestal MJ, Chen W. A split Hopkinson pressure bar technique to determine compressive stress-strain
- 29 data for rock materials. *Exp Mech.* 2001;41(1):40-46.
- 30 Frew DJ, Forrestal MJ, Chen W. Pulse shaping techniques for testing brittle materials with a split Hopkinson

- 1 pressure bar. *Exp Mech.* 2002;42(1):93-106.
- Gary G, Bailly P. Behaviour of quasi-brittle material at high strain rate. Experiment and modelling. *Eur J Mech A Solids*. 1998;17(3):403-420.
- Gran JK, Florence AL, Colton JD. Dynamic triaxial tests of high-strength concrete. *J Eng Mech.* 1989;115(5):891-904.
- Goldsmith W, Sackman JL, Ewerts C. Static and dynamic fracture strength of barre granite. *Int J Rock Mech Min* Sci. 1976;13(11):303-309.
- Hokka M, Black J, Tkalich D, Fourmeau M, Kane A, Hoang NH, Li CC, Chen WW, Kuokkala VT. Effects of strain rate and confining pressure on the compressive behavior of Kuru granite. *Int J Impact Eng.* 2016;91:183-193.
- Ju Y, Sudak L, Xie HP. Study on stress wave propagation in fractured rocks with fractal joint surfaces. *Int J Solids*Struct. 2007;44(13):4256-4271.
- Karinski YS, Zhutovsky S, Feldgun VR, Yankelevsky DZ. The equation of state of unsaturated cementitious composites–A new multiscale model. *Int J Solids Struct.* 2017;109:12-21.
- 14 Kolsky H. Stress waves in solids. Courier Corporation. 1963.
- 15 Kumar A. The effect of stress rate and temperature on the strength of basalt and granite. *Geophysics*. 1968;33(3): 501-510.
- 17 Kumari WGP, Ranjith PG, Perera MSA, Shao S, Chen BK, Lashin A, Arifi N Al, Rathnaweera TD. Mechanical 18 behaviour of Australian Strathbogie uranite under in-situ stress and temperature conditions: An application to 19 geothermal energy extraction. *Geothermics*, 2017;65:44-59.
- 20 Lambert DE, Ross CA. Strain rate effects on dynamic fracture and strength. *Int J Impact Eng.* 2000;24(10):985-998.
- Li JC, Li NN, Li HB, Zhao J. An SHPB test study on wave propagation across rock masses with different contact area ratios of joint. *Int J Impact Eng.* 2017a;105:109-116.
- Li XB, Lok TS, Zhao J. Dynamic characteristics of granite subjected to intermediate loading rate. *Rock Mech Rock* Eng. 2005; 381:21-39.
- Li XB, Zhou T, Li DY. Dynamic strength and fracturing behavior of single-flawed prismatic marble specimens under impact loading with a Split-Hopkinson pressure bar. *Rock Mech Rock Eng.* 2017b;50(1):29-44.
- Li XB, Zhou ZL, Hong L, Yin TB. Large diameter SHPB tests with a special shaped striker. ISRM News J. 2009;
   12:76-79.
- Li XB, Zhou ZL, Lok TS, Hong L, Yin TB. Innovative testing technique of rock subjected to coupled static and dynamic loads. *Int J Rock Mech Min Sci.* 2008; 45(5):739-748.
- Lindholm US, Yeakley LM, Nagy A. The dynamic strength and fracture properties of dresser basalt. *Int J Rock Mech Min Sci.* 1974;115:181-191.
- Liu K, Zhang QB, Wu G, Li JC, Zhao J. Dynamic mechanical and fracture behaviour of sandstone under multiaxial loads using a triaxial Hopkinson bar. *Rock Mech Rock Eng.* 2019;52(7):2175-2195.
- Lu YB, Li QM, Ma GW. Numerical investigation of the dynamic compressive strength of rocks based on split Hopkinson pressure bar tests. *Int J Rock Mech Min Sci.* 2010;54(7):829-838.
- Luo W, Chau VT, Bažant ZP. Effect of high-rate dynamic comminution on penetration of projectiles of various velocities and impact angles into concrete. *Int J Fract.* 2019;216(2):211-221.
- Melosh HJ, Ryan EV, Asphaug E. Dynamic fragmentation in impacts: Hydrocode simulation of laboratory impacts. *J Geophys Res Planets*. 1992;97(E9):14735-14759.
- 41 Nemat-Nasser S, Isaacs J, Rome J. Triaxial Hopkinson techniques. Materials Park. OH: ASM International,

- 1 2000:516-518.
- Nie HL, Suo T, Wu BB, Li YL, Zhao H. A versatile split Hopkinson pressure bar using electromagnetic loading. *Int J Impact Eng.* 2018a;116:94-104.
- Nie HL, Suo T, Shi XP, Liu HF, Li YL, Zhao H. Symmetric split Hopkinson compression and tension tests using synchronized electromagnetic stress pulse generators. *Int J Impact Eng.* 2018b;122:73-82.
- Olsson WA. The compressive strength of tuff as a function of strain rate from 10<sup>-6</sup> to 10<sup>3</sup>/sec. *Int J Rock Mech Min Sci.* 1991;28(1):115-118.
- Patton TL, Logan JM, Friedman M. Experimentally generated normal faults in single-layer and multilayer limestone specimens at confining pressure. *Tectonophysics*. 1998;295(1-2):53-77.
- Peng K, Liu ZP, Zou QL, Zhang ZZ, Zhou JQ. Static and dynamic mechanical properties of granite from various burial depths. *Rock Mech Rock Eng.* 2019;52(10):3545-3566.
- Peng RD, Ju Y, Wang JG, Xie HP, Gao F, Mao LT. Energy dissipation and release during coal failure under conventional triaxial compression. *Rock Mech Rock Eng.* 2015;48(2):509-526.
- Perkins RD, Green SJ, Friedman M. Uniaxial stress behavior of porphyritic tonalite at strain rates to 10<sup>3</sup>/second. *Int J Rock Mech Min Sci.* 1970;75:527-535.
- Qi CZ, Xia C, Li XZ, Sun YJ. Effect of inertia and crack propagation on dynamic strength of geologic-type materials. *Int J Impact Eng.* 2019;133:103367.
- Ranjith PG, Zhao J, Ju M, De Silva RV, Rathnaweera TD, Bandara AK. Opportunities and challenges in deep mining:

  A brief review. *Engineering*. 2017;3(4):546-551.
- 20 Reddish DJ, Stace LR, Vanichkobchinda P, Whittles DN. Numerical simulation of the dynamic impact breakage testing of rock. *Int J Rock Mech Min Sci.* 2005;42(2):167-176.
- Rehbock-Sander M, Jesel T. Fault induced rock bursts and micro-tremors—experiences from the Gotthard base tunnel. *Tunn Undergr Space Technol.* 2018;81:358-366.
- Richter B, Stünitz H, Heilbronner R. The brittle-to-viscous transition in polycrystalline quartz: An experimental study. *J Struct Geol.* 2018;114:1-21.
- Scott TE, Nielsen KC. The effects of porosity on the brittle-ductile transition in sandstones. *J Geophys Res Solid Earth.* 1991;96(B1):405-414.
- Song B, Chen W. Loading and unloading split Hopkinson pressure bar pulse-shaping techniques for dynamic hysteretic loops. *Exp Mech.* 2004;44(6):622-627.
- Wang M, Zhu ZM, Dong YQ, Zhou L. Study of mixed-mode I/II fractures using single cleavage semicircle compression specimens under impacting loads. *Eng Fract Mech.* 2017;177:33-44.
- Wang QZ, Li W, Xie HP. Dynamic split tensile test of flattened Brazilian disc of rock with SHPB setup. *Mech Mater.* 2009;41(3):252-260.
- Wasantha PL, Ranjith PG. Water-weakening behavior of Hawkesbury sandstone in brittle regime. *Eng Geol.* 2014;178:91-101.
- Whittles DN, Kingman S, Lowndes I, Jackson K. Laboratory and numerical investigation into the characteristics of rock fragmentation. *Miner Eng.* 2006;19(14):1418-1429.
- Wu BB, Yao W, Xia KW. An experimental study of dynamic tensile failure of rocks subjected to hydrostatic confinement. *Rock Mech Rock Eng.* 2016;49(10):3855-3864.
- 40 Xia KW, Yao W. Dynamic rock tests using split Hopkinson Kolsky bar system—A review. *J Rock Mech Geotech*41 Eng. 2015;7(1):27-59.

- 1 Xie HP, Sanderson DJ. Fractal effects of crack propagation on dynamic stress intensity factors and crack velocities. *Int J Fract.* 1996;74(1):29-42.
- 3 Xie HP, Zhu JB, Zhou T, Zhang K, Zhou CT. Conceptualization and preliminary study of engineering disturbed 4 rock dynamics. *Geomech. Geophys Geo-energ Geo-resour.* 2020;6:34.
- Xie HP, Zhu JB, Zhou T, Zhao J. Novel three-dimensional rock dynamic tests using the true triaxial electromagnetic Hopkinson bar system. *Rock Mech Rock Eng.* 2021;54:2079-2086.
- Xu SL, Shan JF, Zhang L, Zhou LJ, Gao GF, Hu SS, Wang PF. Dynamic compression behaviors of concrete under true triaxial confinement: An experimental technique. *Mech Mater.* 2020;140:103220.
- 9 Yuan FP, Prakash V, Tullis T. Origin of pulverized rocks during earthquake fault rupture. *J Geophys Res Solid* 10 *Earth*. 2011;116(B06309):1-18.
- Zhang QB, Zhao J. Determination of mechanical properties and full-field strain measurements of rock material under dynamic loads. *Int J Rock Mech Min Sci.* 2013;60:423-439.
- Zhang QB, Zhao J. A review of dynamic experimental techniques and mechanical behaviour of rock materials. *Rock Mech Rock Eng.* 2014;47(4):1411-1478.
- Zhao H, Gary G. On the use of SHPB techniques to determine the dynamic behavior of materials in the range of
   small strains. *Int J Solids Struct.* 1996;33(23):3363-3375.
- Zhao J, Cadoni E. Triaxially compressed Hopkinson bar (TriHB) for geomaterial and construction material
   testing. Proposal Submitted to the Swiss National Science Foundation (SNSF), 2009, No. 206021\_128734,
   EPFL, Switzerloand.
- Zhao J, et. al., Three dimensionally compressed and monitored Hopkinson bar. Australian Research Council, ARC
   LIEF (No. LE150100058), 2015, granted in 2016, Monash University, Australia.
- Zhou YX, Xia KW, Li XB, Li HB, Ma GW, Zhao J, Zhou ZL, Dai F. Suggested methods for determining the dynamic
   strength parameters and mode-I fracture toughness of rock materials. *Int J Rock Mech Min Sci.* 2012;49:105 112.
- Zhou T, Dong SL, Zhao GF, Zhang R, Wu SY, Zhu JB. An experimental study of fatigue behavior of granite under
   low-cycle repetitive compressive impacts. *Rock Mech Rock Eng.* 2018;51(10):3157-3166.
- Zhou T, Zhu JB, Xie HP. Mechanical and volumetric fracturing behaviour of three-dimensional printing rock-like
   samples under dynamic loading. *Rock Mech Rock Eng.* 2020;53:2855-2864.
- Zhu JB, Liao ZY, Tang CA. Numerical SHPB tests of rocks under combined static and dynamic loading conditions
   with application to dynamic behavior of rocks under in situ stresses. *Rock Mech Rock Eng.* 2016;49(10):3935-31
   3946.
- Zhu JB, Zhou T, Liao ZY, Sun L, Li XB, Chen R. Replication of internal defects and investigation of mechanical and fracture behaviour of rock using 3D printing and 3D numerical methods in combination with X-ray computerized tomography. *Int J Rock Mech Min Sci.* 2018a;106:198-212.



**Fig. 1** Dynamic true triaxial electromagnetic Hopkinson bar (DTEHB) system: (a) Overall system configuration; (b) Three key components of the 3D centering and leveling system

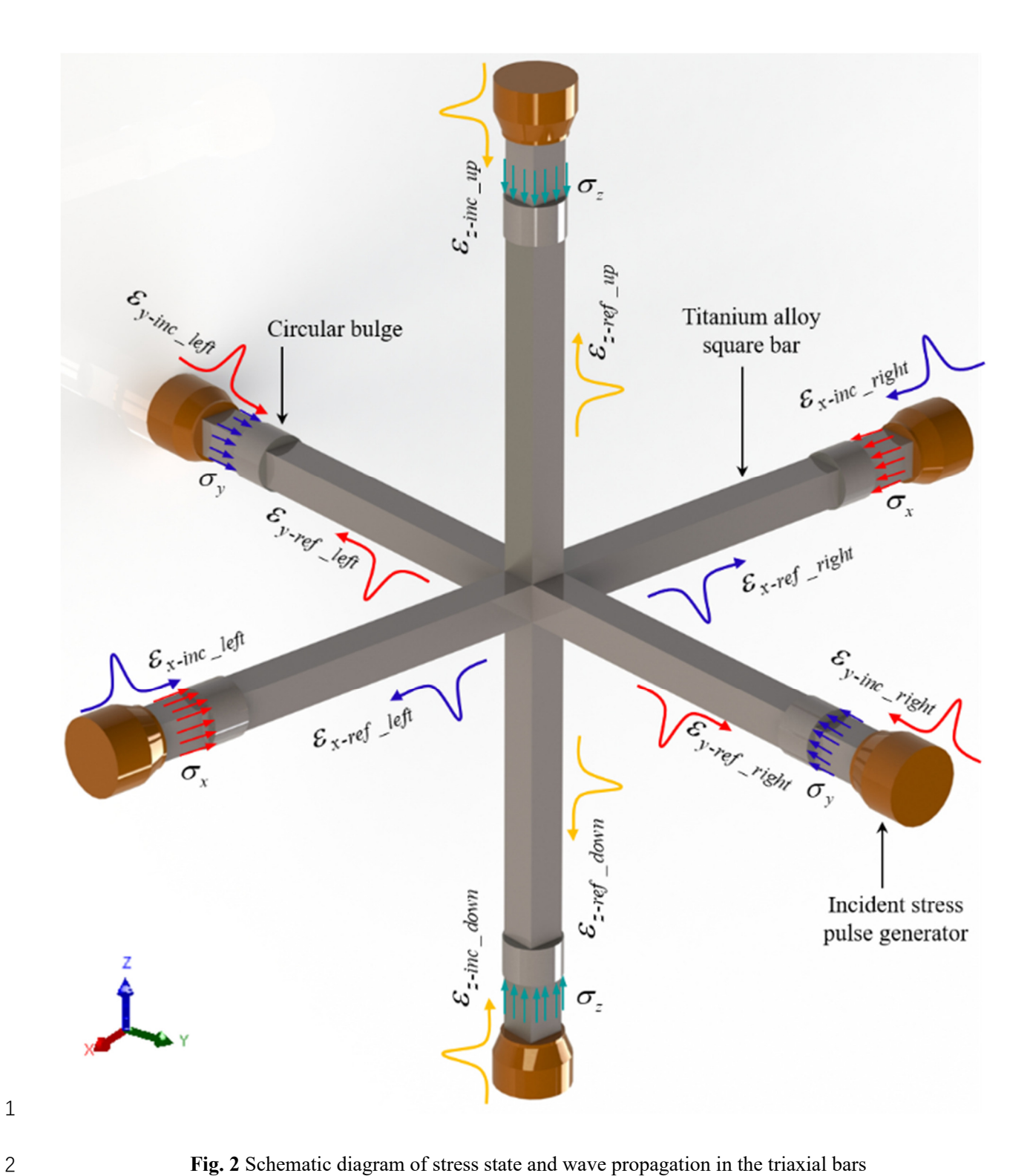


Fig. 2 Schematic diagram of stress state and wave propagation in the triaxial bars

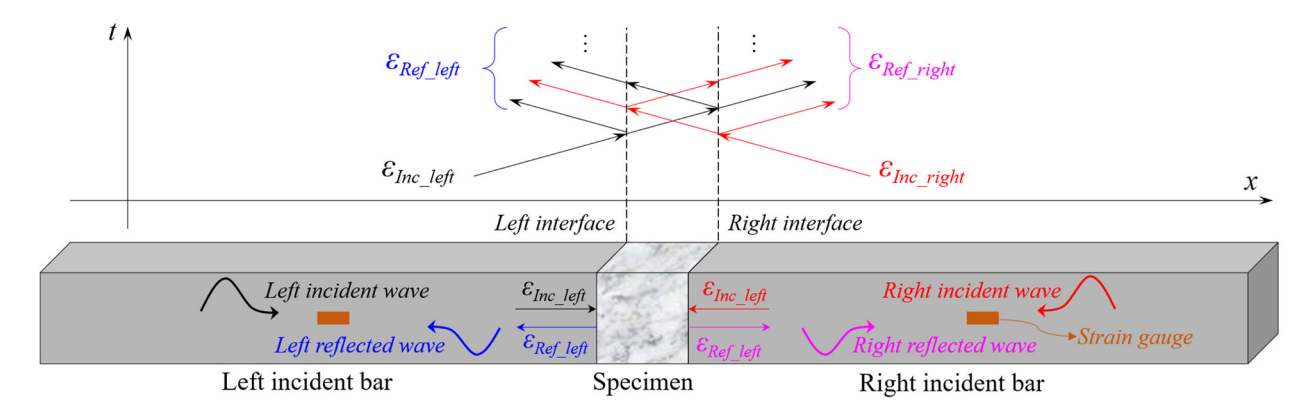


Fig. 3 Schematic diagram of wave propagation along the x-axis under conditions of symmetric loading

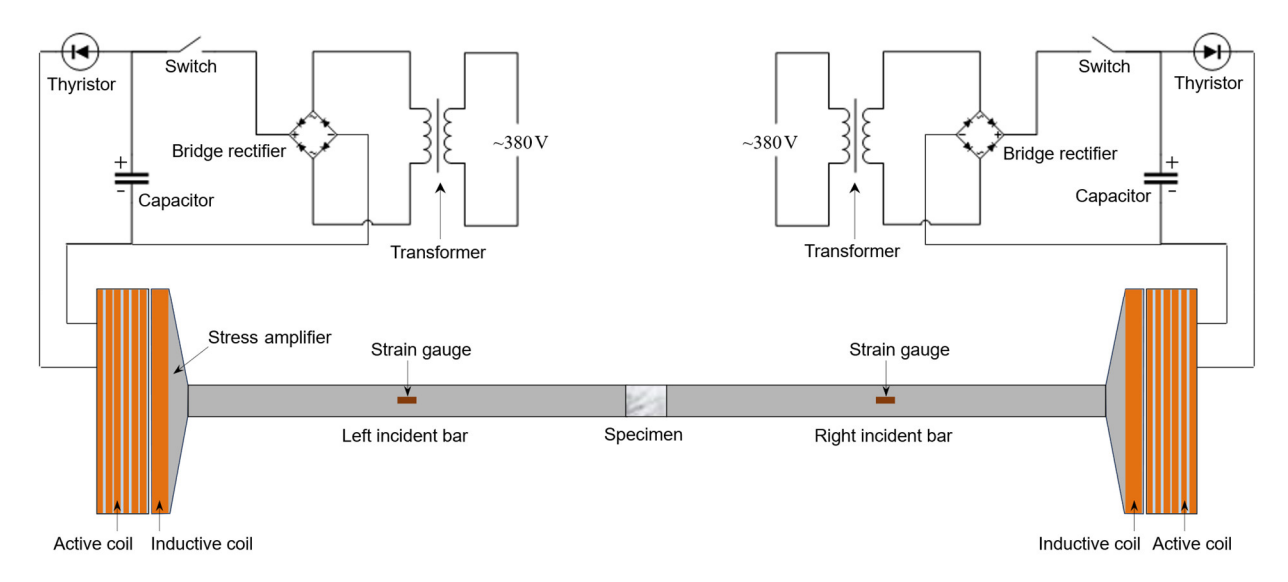


Fig. 4 Schematic diagram of electromagnetic stress pulse generation system in each axis

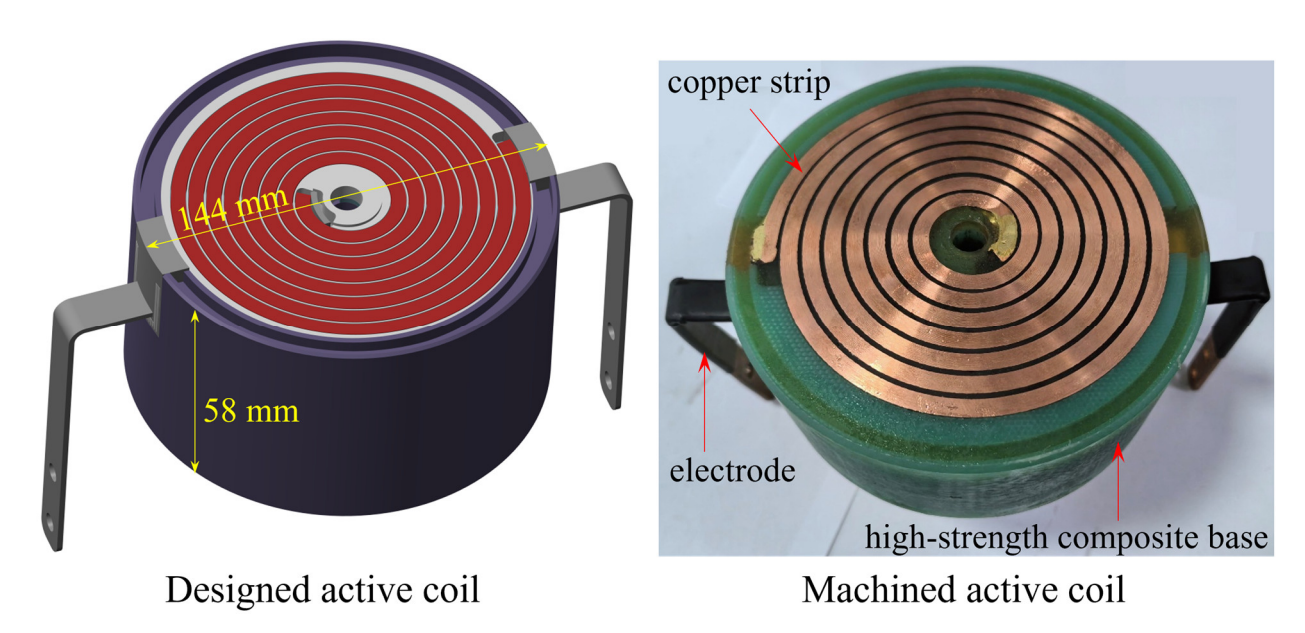
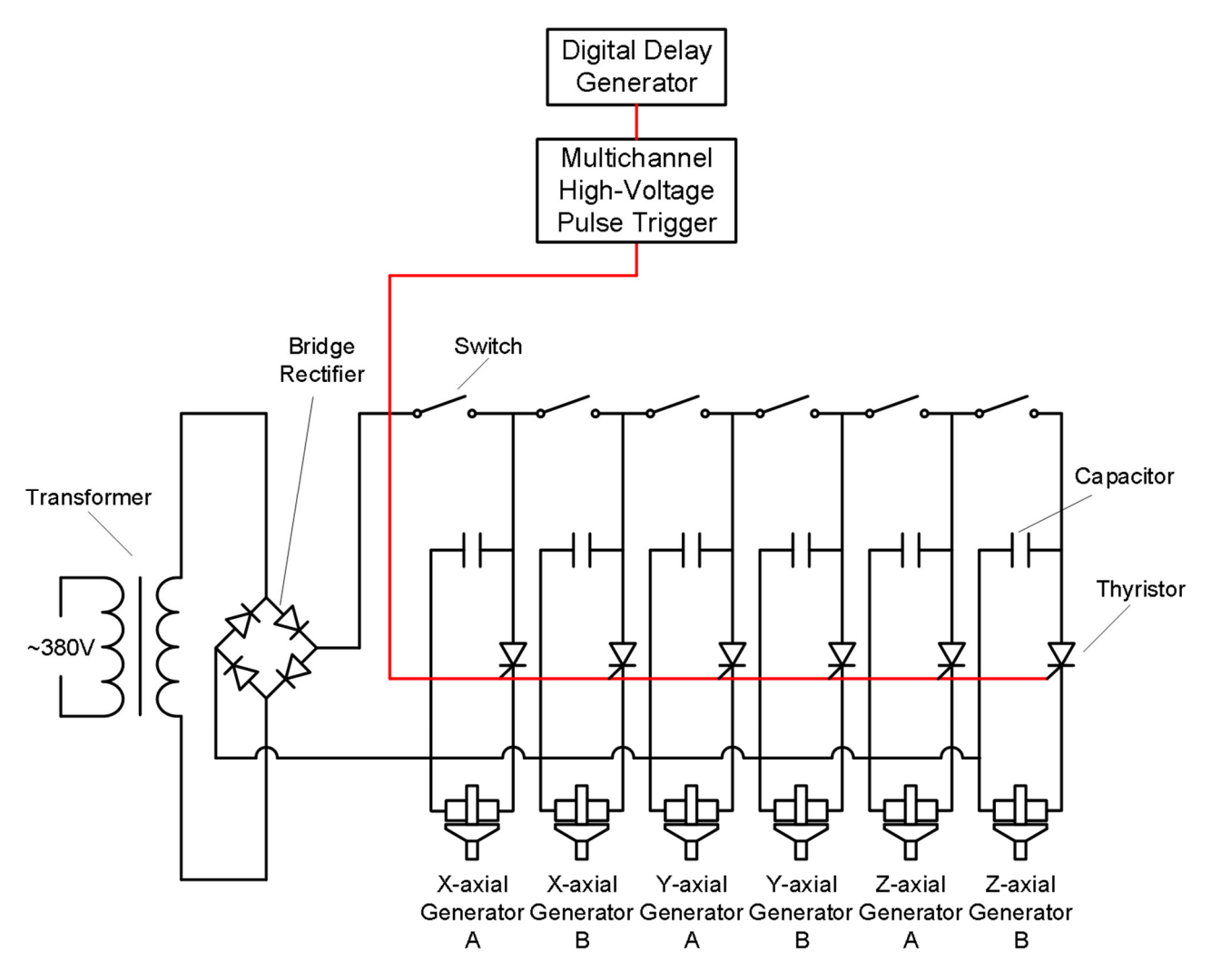


Fig. 5 3D structure of an active coil



 $\textbf{Fig. 6} \ \textbf{Schematic diagram of the synchronous pulse control system}$ 

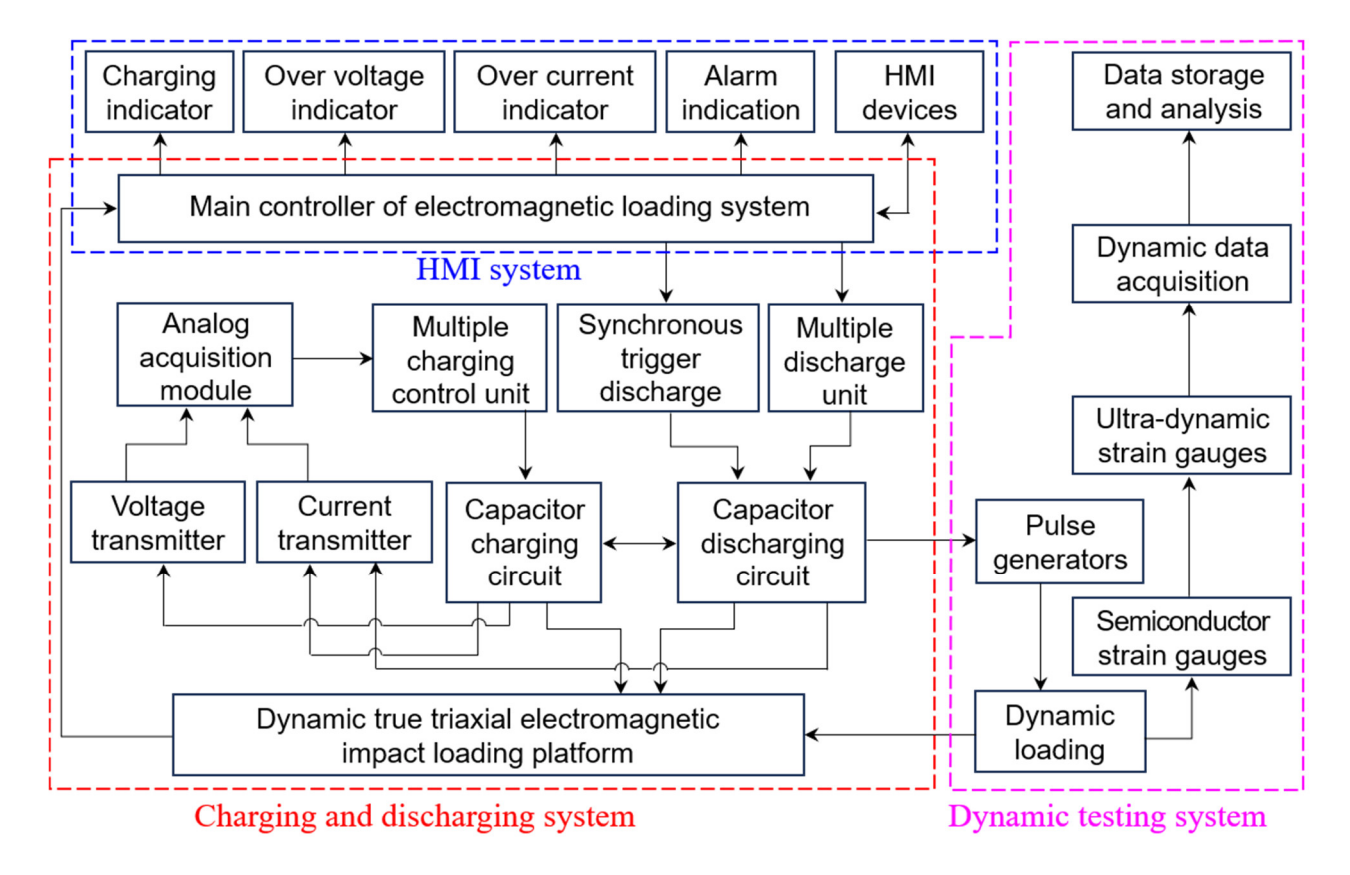


Fig. 7 Principle of the central control system

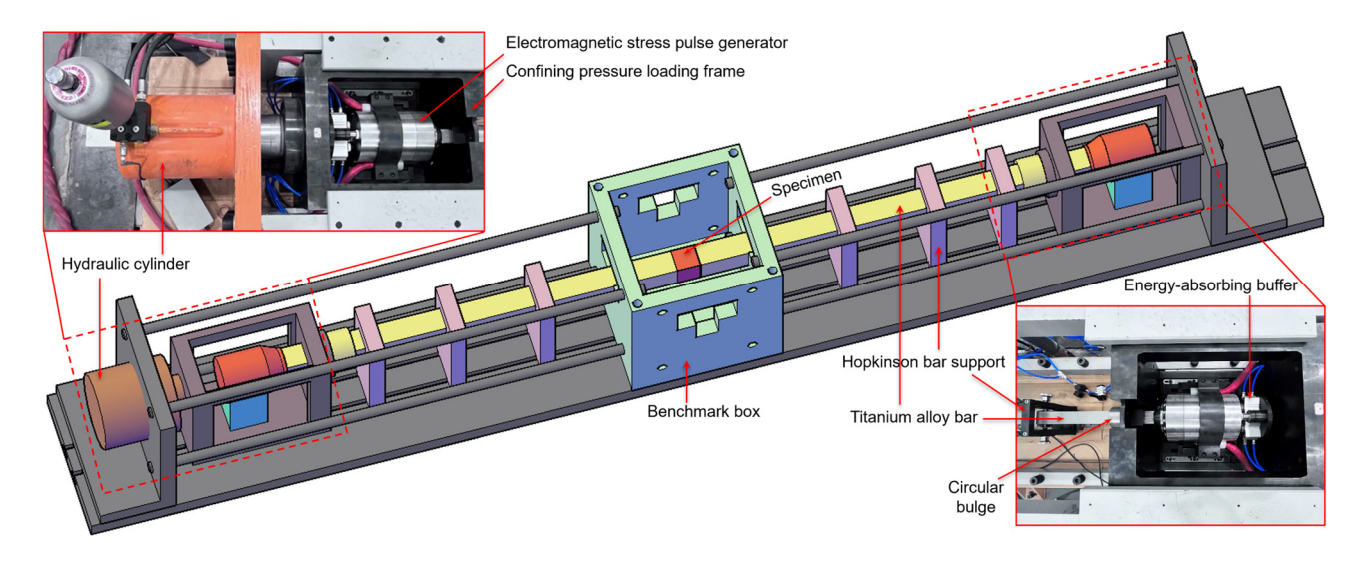


Fig. 8 Primary structural frame and static confining pressure loading system in one axis

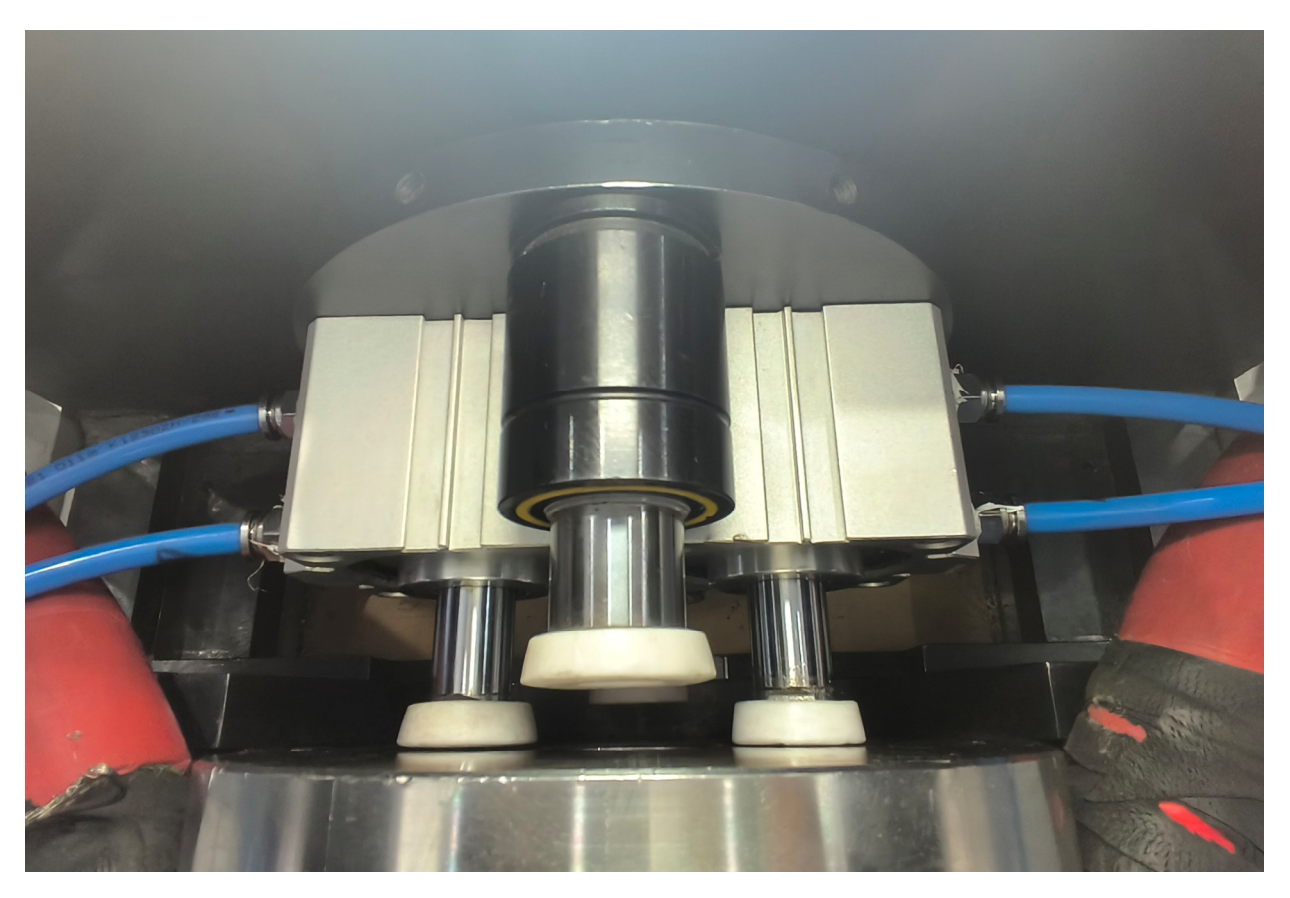


Fig. 9 Energy-absorbing buffer with self-resetting capability

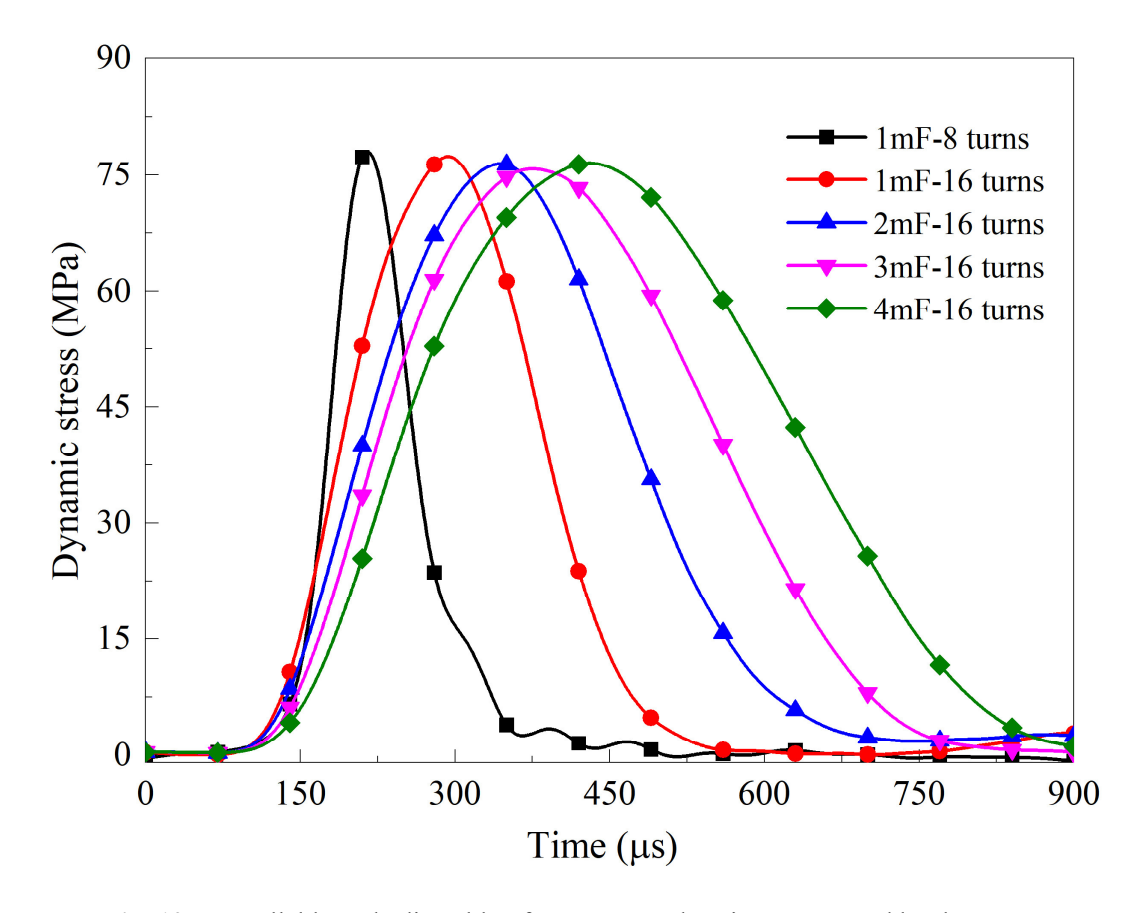
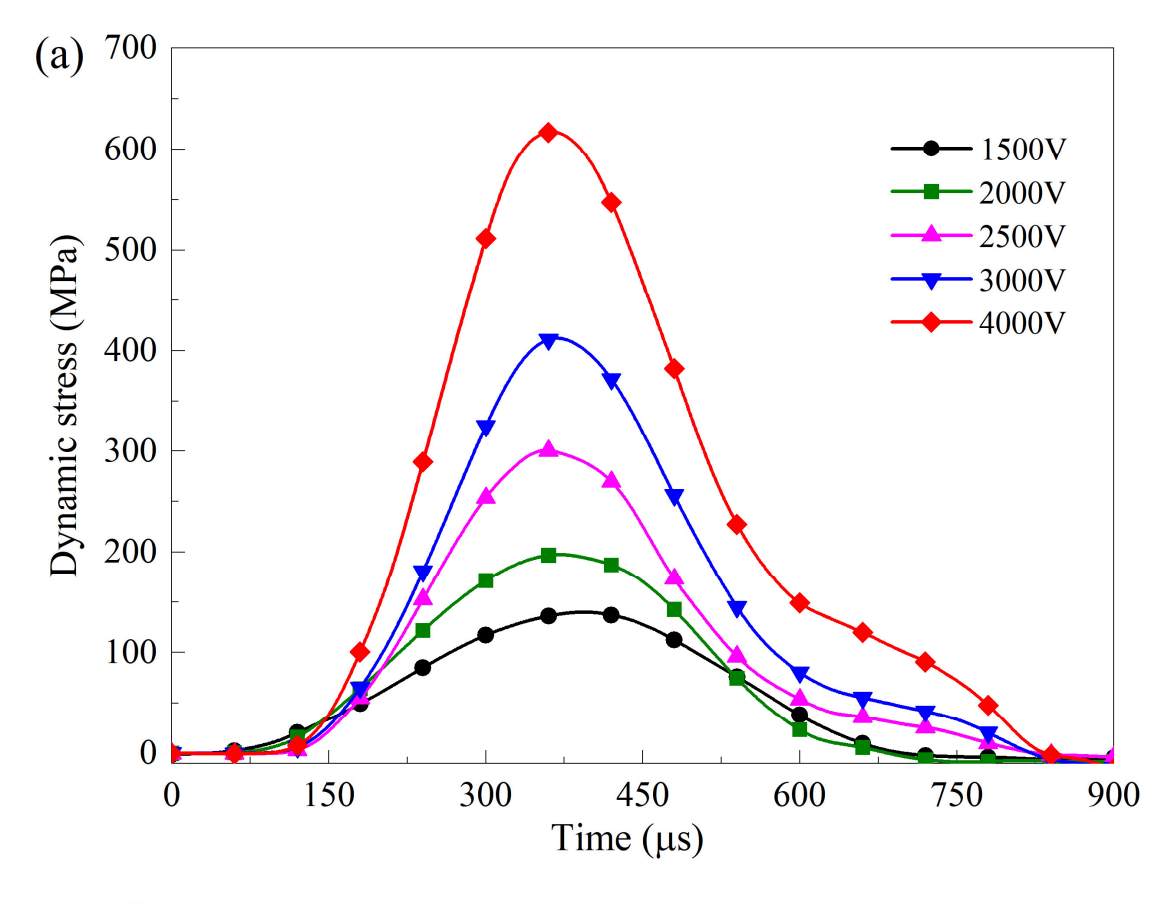
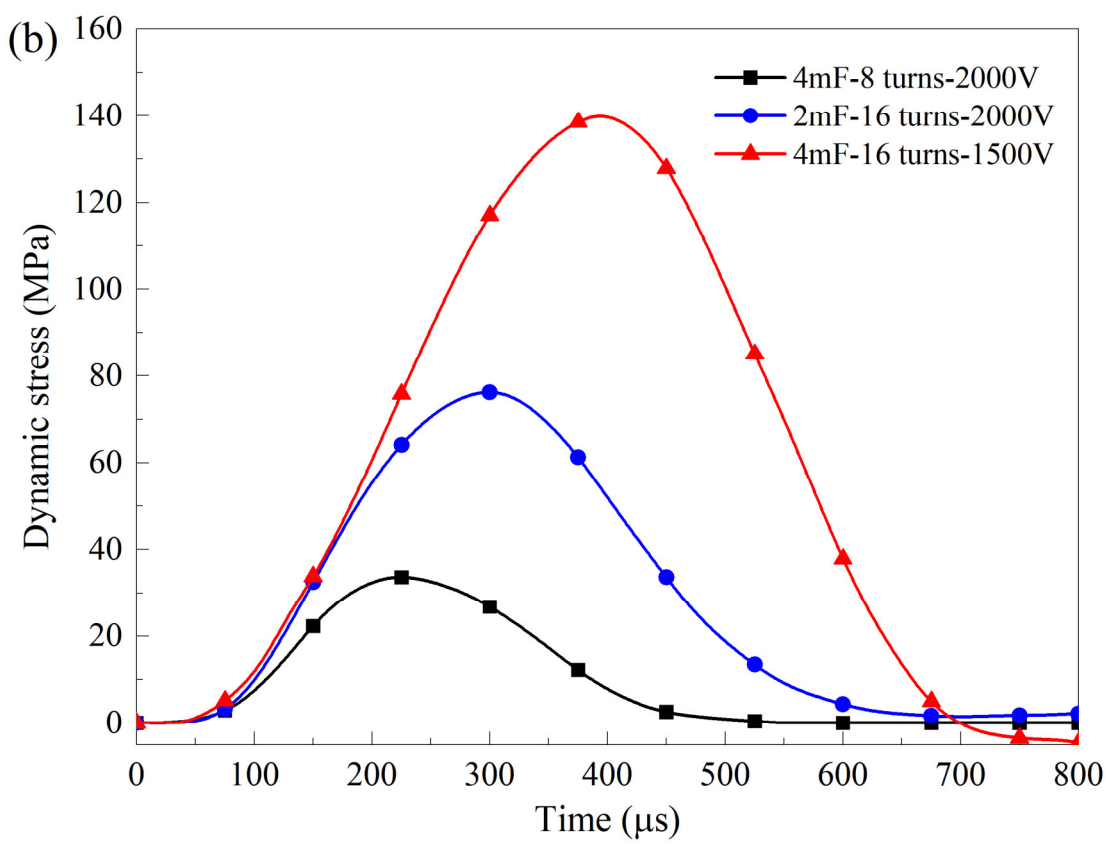


Fig. 10 Controllable and adjustable of stress wave durations generated by the ESPG





**Fig. 11** Controllable and adjustable of stress wave amplitudes generated by the ESPG. (a) Effect of charging voltages on stress wave amplitude; (b) Influence of capacitance and active coil turns on stress wave amplitude.

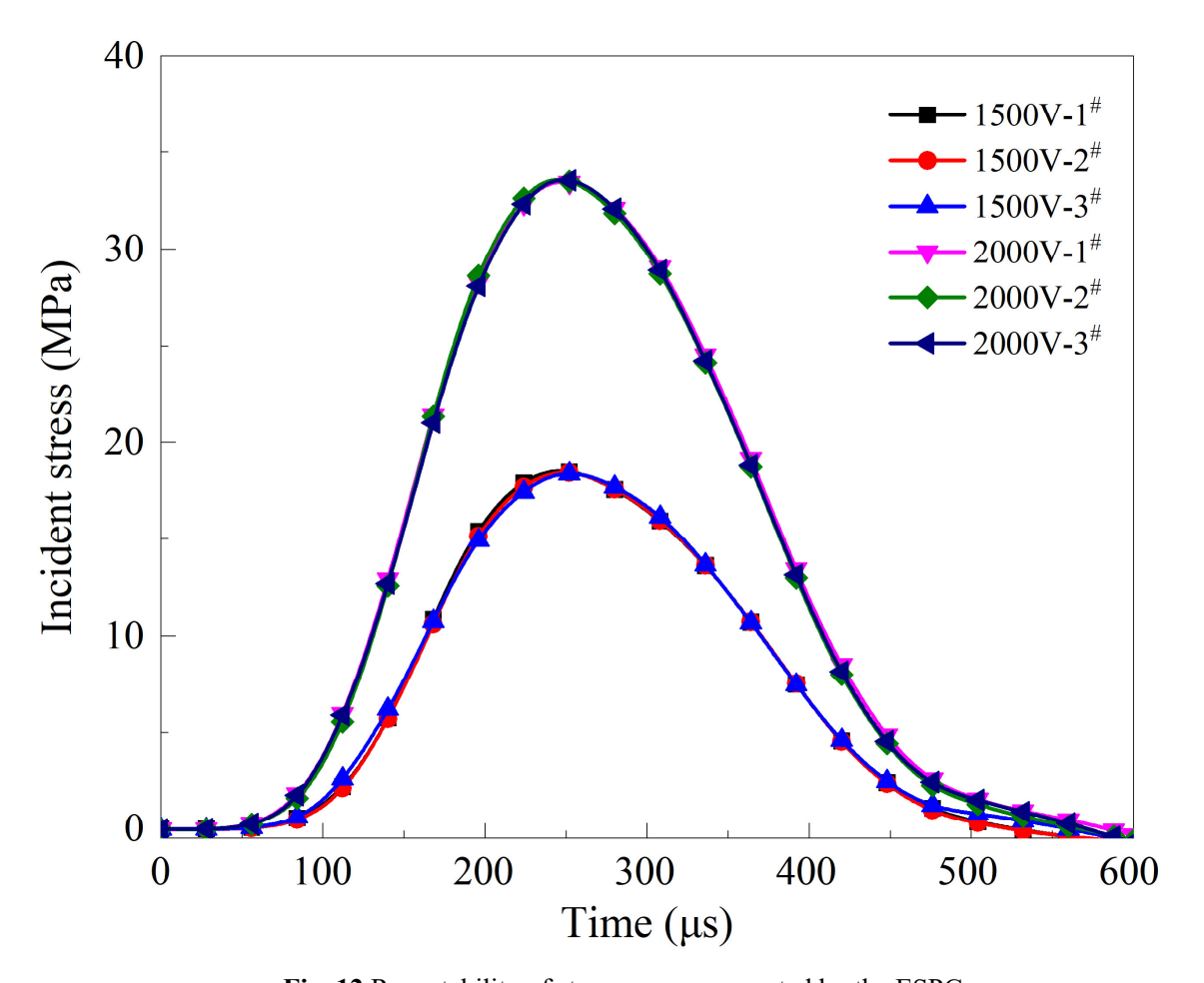


Fig. 12 Repeatability of stress waves generated by the ESPG

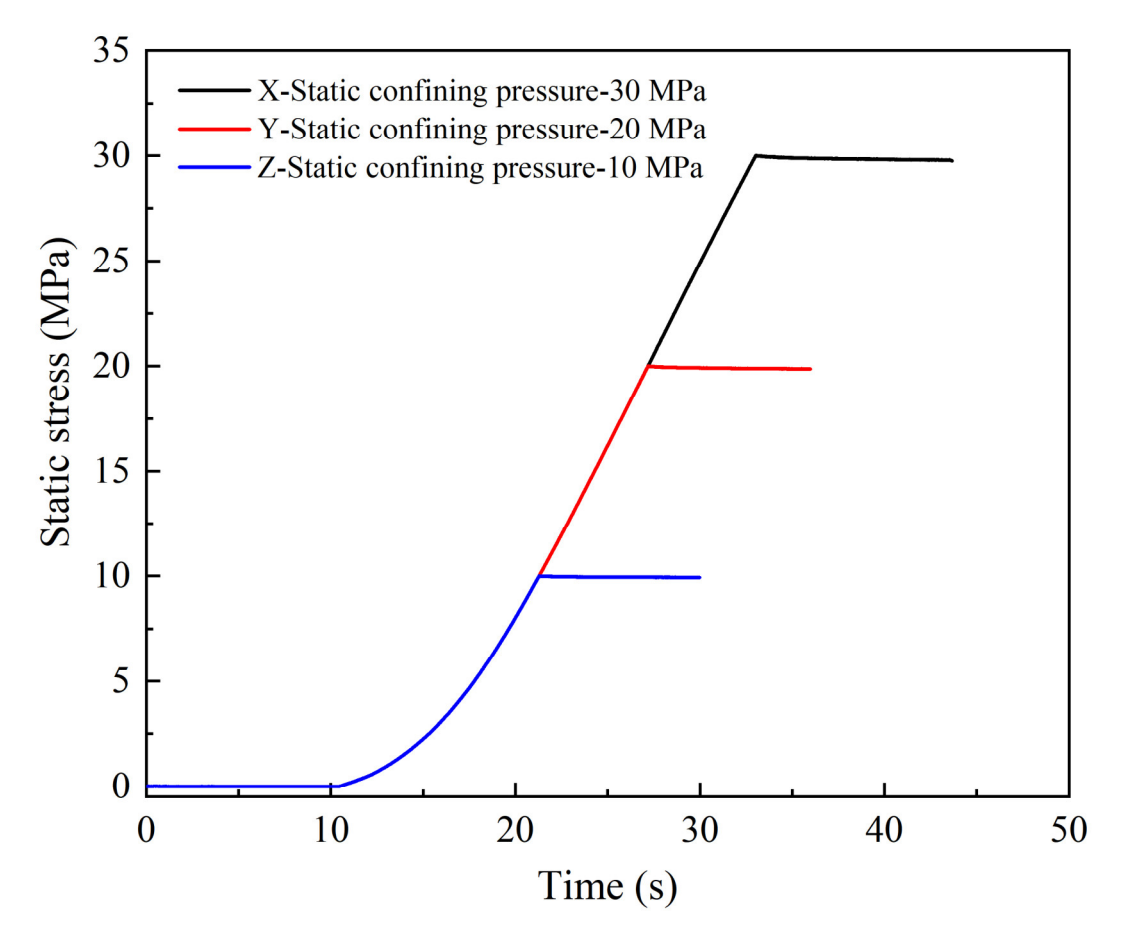
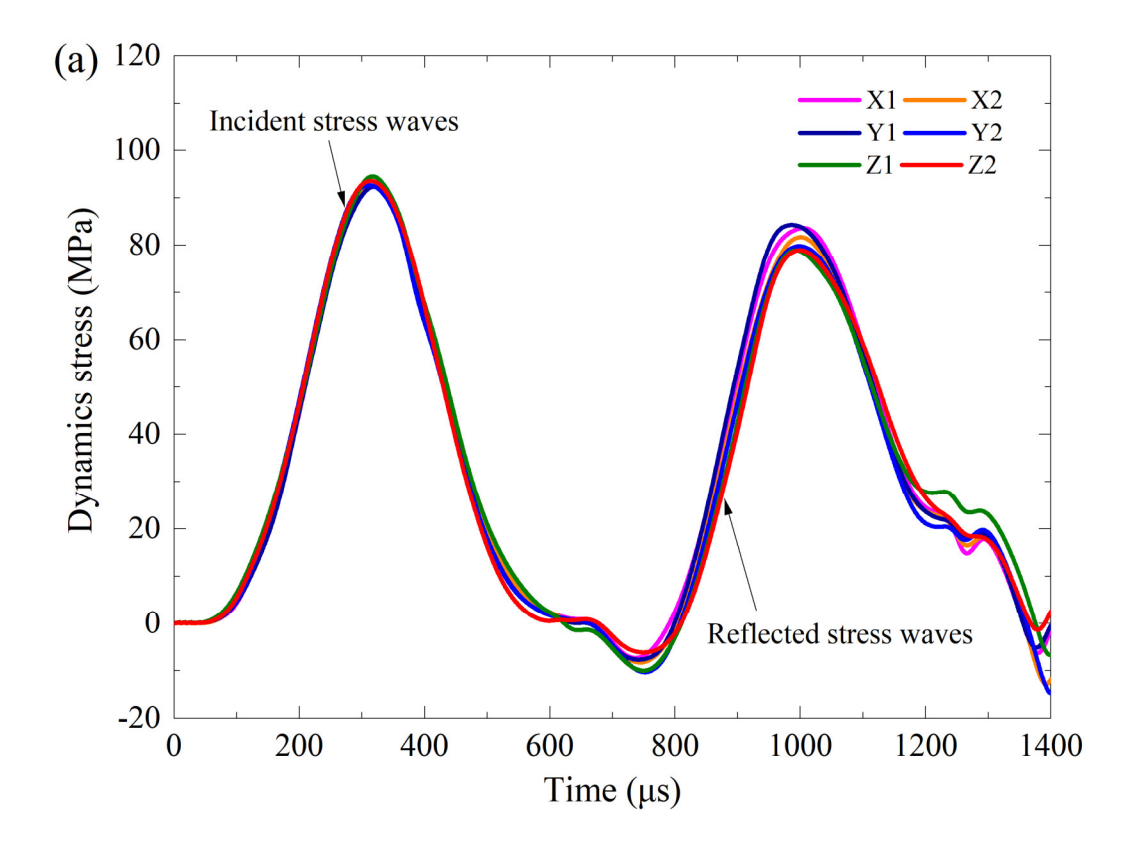
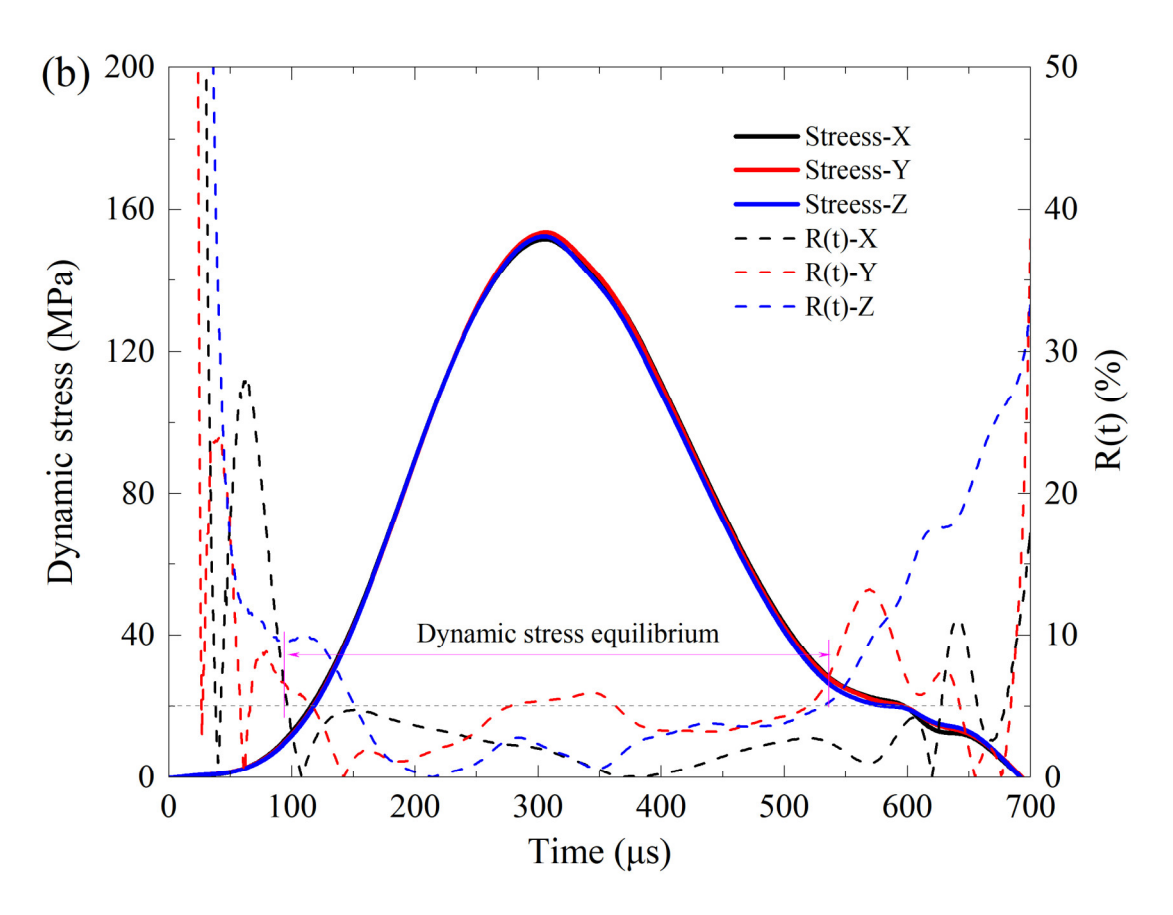
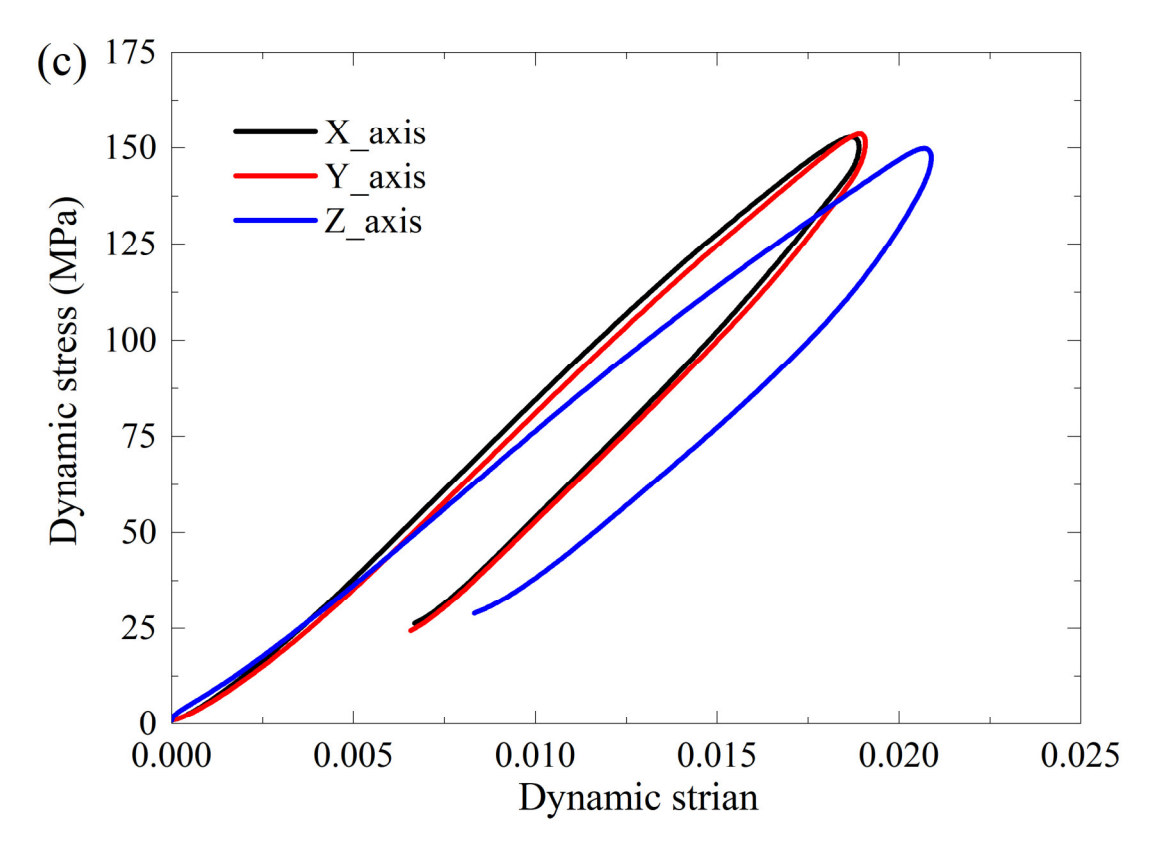


Fig. 13 Application of static confining pressures along each axis







**Fig. 14** A typical dynamic true triaxial impact test of a coal specimen. (a) Incident strain signals measured on the triaxial bars; (b) Dynamic stress balance in each axis; (c) Dynamic stress-strain curves in the X, Y and Z axes of the coal specimen.

Table 1 Summary of the techniques, equipment and objectives for data acquisition and analysis

Signals	Technique	Equipment	Objectives
Dynamic strain	Synchronous signal acquisition technology	Multi-channel dynamic strain recorder	To derive dynamic stress-strain curves; analyzing dynamic mechanical properties, e.g., dynamic strength and strain
Surface fracturing	High-speed photogrammetry	Ultra-high-speed camera	To obtain crack propagation velocity; analyzing crack nucleation, initiation, propagation, coalescence and failure modes
3D fracturing, deformation	High-speed photogrammetry, 3D DIC technique	High-speed cameras, DIC analysis software	To analyze 3D fracturing type, behavior and mechanism; analyzing full field deformation and its localization and evolution
Surface temperature evolution	High-speed infrared thermography	High-speed infrared thermal camera	To characterize rock fracture thermomechanics; analyzing real- time temperature evolution, fracture-zone thermal fields, and energy dissipation
Acoustic emission (AE)	AE detection technology	AE probe, AE detector	To analyze dynamic damage and fracturing mode of the specimen
Macro- and meso- cracks	X-ray computed tomography (CT)	High-resolution X-ray CT	2D and 3D damage and fracture network inside opaque materials; spatial evolution of micro- and macro-crack inside the specimen
Meso- and micro-cracks	Scanning electron microscope	Scanning electron microscope	Microcrack characteristics; failure mechanism of the specimen at microscopic scale